



A contact domain method for large deformation frictional contact problems. Part 1: Theoretical basis

J. Oliver^{a,*}, S. Hartmann^a, J.C. Cante^b, R. Weyler^b, J.A. Hernández^a

^aE.T.S. d'Enginyers de Camins, Canals i Ports, Technical University of Catalonia (UPC), Campus Nord UPC, Mòdul C-1, c/Jordi Girona 1-3, 08034 Barcelona, Spain

^bE.T.S. d'Enginyeria Industrial i Aeronàutica de Terrassa, Technical University of Catalonia (UPC), Campus Nord UPC, Mòdul C-1, c/Jordi Girona 1-3, 08034 Barcelona, Spain

ARTICLE INFO

Article history:

Received 7 August 2008

Received in revised form 6 March 2009

Accepted 10 March 2009

Available online 21 March 2009

Keywords:

Contact mechanics
Lagrange multipliers
Contact domain method
Interior penalty method
Nitsche method
Friction
Active set strategy

ABSTRACT

In the first part of this work, the theoretical basis of a frictional contact domain method for two-dimensional large deformation problems is presented. Most of the existing contact formulations impose the contact constraints on the boundary of one of the contacting bodies, which necessitates the projection of certain quantities from one contacting surface onto the other. In this work, the contact constraints are formulated on a so-called contact domain, which has the same dimension as the contacting bodies. This contact domain can be interpreted as a fictive intermediate region connecting the potential contact surfaces of the deformable bodies. The introduced contact domain is subdivided into a non-overlapping set of patches and is endowed with a displacement field, interpolated from the displacements at the contact surfaces. This leads to a contact formulation that is based on dimensionless, strain-like measures for the normal and tangential gaps and that exactly passes the contact patch test. In addition, the contact constraints are enforced using a stabilized Lagrange multiplier formulation based on an interior penalty method (Nitsche method). This allows the condensation of the introduced Lagrange multipliers and leads to a purely displacement driven problem. An active set strategy, based on the concept of effective gaps as entities suitable for smooth extrapolation, is used for determining the active normal stick and slip patches of the contact domain.

© 2009 Elsevier B.V. All rights reserved.

1. Motivation

Despite the substantial progress achieved in the last years, simulating technical problems involving contact of various deformable parts still poses challenges in non-linear structural mechanics, mainly when it is intended to obtain robust and accurate results at a reduced computational cost using implicit methods. For the development of a contact formulation, two main ingredients may be basically chosen:

- A scheme to enforce the contact constraints.
- A technique to discretize the contact surfaces or the interface.

Several different methods for the variational enforcement of the contact constraints have been developed in the past. The most prominent of them are: (a) the penalty method, (b) the Lagrange multiplier method and (c) the augmented Lagrange method. These methods have been used together with specific collocation methods to enforce the contact constraints at some discrete nodal points (e.g. [13,21,25,29]), as well as with discretization schemes based on a continuous treatment of the contact constraints (e.g.

[20,24,32]). An overview of various methods for the contact constraint enforcement with respect to different discretization strategies is given in Wriggers [27]. Recently a different approach based on a formulation for the matching of different meshes, introduced by Nitsche [19], was utilized for the formulation of frictionless, small deformation contact problems by Wriggers and Zavarise [30]. Instead of introducing a Lagrange multiplier, the calculation of the stresses in the contact interface is based on the stress field of the contacting bodies. The formulation necessitates a stabilization term, which looks very similar to the penalty method, but exhibits less influence on the solution than the classical penalty approach. Another approach based on the Nitsche method was introduced by Heintz and Hansbo [14] for small deformation frictional contact problems. Starting from a classical Lagrange multiplier method, they introduce a stabilization term, connecting the Lagrange multipliers with the stress field of the contacting bodies at the contact boundary, in order to be able to condense the introduced Lagrange multipliers. In this work, the formulation presented in [14] is generalized to the contact domain method for large deformation frictional contact problems.

Many existing contact formulations developed in the past enforce the contact constraints at specific collocation points. The most popular discretization strategy in the context of large deformation contact problems is the node-to-segment approach

* Corresponding author.

E-mail address: xavier.oliver@upc.edu (J. Oliver).

developed by Hallquist et al. [11]. Its main idea is that a specific node on the slave side must not penetrate the opposing master side segment. This approach can be applied in a single pass algorithm, where only nodes on the slave side are checked against penetration into the master segment, and the nodes on the master side are free to penetrate the slave segments. As the single pass method does not pass the contact patch test [7,20], the so-called two pass algorithm displays an alternative for the simulation of flexible body contact. The two pass algorithm performs the nodal contact search twice and solves the contact patch test in 2D, but it is prone to lock due to overconstraining of the displacements on the contact surface. In recent years other discretization schemes were developed, based on a continuous treatment of the contact constraints. Many of the lately proposed segment-to-segment discretization strategies are based on the so-called mortar method, initially introduced in the context of domain decomposition methods [3–5]. This method is particularly well suited to exchange information of two discretized domains along common, in general non-conforming, surface grids. In contrast to the node-to-segment discretization, the continuity constraints are not enforced at discrete nodal points but are formulated along the entire coupling boundary in a weak integral sense. On basis of the mortar method, various contact formulations have been developed in recent years. For a more mathematical treatment the works of Belgacem et al. [2], Hild [15], Wohlmuth and Krause [26] or Hübner and Wohlmuth [16] may be named. Furthermore several approaches in the engineering community appeared recently, e.g. Yang et al. [31], Puso and Laursen [22,23], Fischer and Wriggers [8,9].

No matter whether using a node-to-segment or a segment-to-segment contact discretization strategy, nearly all of the proposed methods have in common, that they project somehow one contact-surface/point (*slave/non-mortar*) onto the other contact-surface (*master/mortar*), to formulate the necessary contact conditions. Therefore, the contact problem is defined on a subdomain, which is usually one dimension lower than the domain of the contacting bodies (see Fig. 1a). In this paper, a so-called *contact domain* is utilized to formulate the contact constraints. It is an intermediate domain of the same dimension than the contacting bodies, which connects potential contact boundaries. The contact domain will be approximated with a set of non-overlapping patches (see Fig. 1b) and endowed with a displacement field, interpolated from the displacements of the boundaries of the contacting bodies. Consequently, the measurements of the normal and tangential gaps as well as the introduced Lagrange multipliers are defined within the whole contact domain, and not only along the contacting surfaces.

This leads to a contact algorithm formulated in terms of dimensionless, strain-like measures based on the incremental motion of the contact domain, for the normal and tangential gaps, whose necessary variations and linearizations can be performed utilizing

standard manipulations of strain measures in classical continuum mechanics.

A key issue of the contact discretization via a contact domain is the fact, that the resulting pairing of the contact surfaces is complete and continuously defined. To illustrate this, Fig. 2 sketches two discretized contact surfaces and its corresponding contact pairings, either with a classical node-to-segment approach with a nodal non-penetration condition (Fig. 2a) or with the contact domain, utilizing triangular patches (Fig. 2b). There, for the node-to-segment pairing two obvious things can be checked: first, it strongly depends on the choice of the master and slave sides and, second, it might discard (void regions in Fig. 2a) or over-constrain (overlapping regions in Fig. 2a) some specific pairings. These facts can pose difficulties to the method to pass the patch test. In contrast, the contact domain displays full and non-overlapping pairings (see Fig. 2b), which, as it will be shown later, lead to a contact algorithm that passes the contact patch test for arbitrary not matching meshes.

This work focuses on a two-dimensional version of the contact domain method in contact problems. This first part deals with the fundamental geometrical, mechanical and mathematical aspects, thus emphasizing the theoretical aspects of the method. The second part [12] is focused on ensuring the reproducibility of the work by fully detailing the numerical and algorithmic aspects of the method and providing a suitable number of assessing examples.

This paper will be organized as follows: In Section 2 the geometrical aspects of the utilized *contact domain*, including necessary definitions for the applied normal and tangential gaps will be specified for the use of linear triangular contact patches. The boundary value problem of the large deformation frictional contact problem as well as the necessary contact constraints are then given in Section 3. Section 4 focuses on the introduction of a stabilized weak form of the boundary value problem as basis for solving it by means of the finite element method. An appropriate active set strategy, based on so-called *effective gaps* and *active set indicators* is presented in Section 5, in order to translate the underlying inequality constrained problem into an equality one. The paper closes with some concluding remarks in Section 6.

2. Geometrical aspects

2.1. Contact domain

Consider two contacting bodies $\mathcal{B}^{(\alpha)}$, $\alpha = 1, 2$, which undergo large deformations (see Fig. 3). Let then $\phi_t^{(\alpha)}(\mathbf{X}) \equiv \phi^{(\alpha)}(\mathbf{X}, t) : \mathcal{B}^{(\alpha)} \times [0, T] \rightarrow \Omega^{(\alpha)}$ denote the associated deformation maps at time $t \in [0, T]$, where $\phi_t^{(\alpha)}$ maps material points $\mathbf{X}^{(\alpha)} \in \mathcal{B}^{(\alpha)}$ at the reference configuration onto points $\mathbf{x}^{(\alpha)} = \phi_t^{(\alpha)}(\mathbf{X}^{(\alpha)})$ at the current configuration. Furthermore the *total displacement field* $\mathbf{U}_t^{(\alpha)}(\mathbf{X}^{(\alpha)})$ is

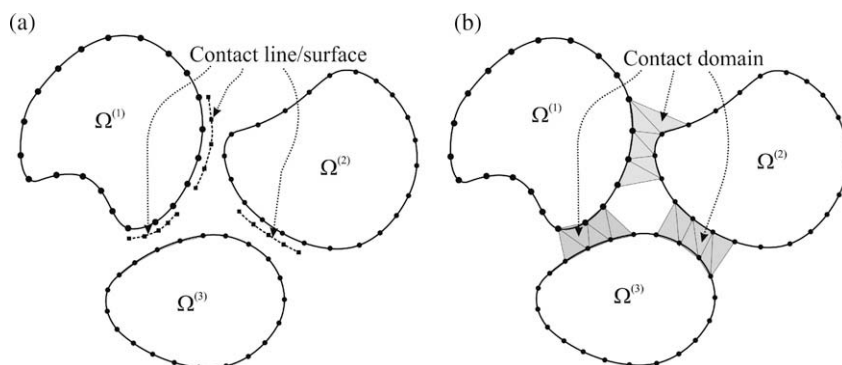


Fig. 1. Imposition of contact constraints on the contacting bodies: (a) classical methods and (b) contact domain method.

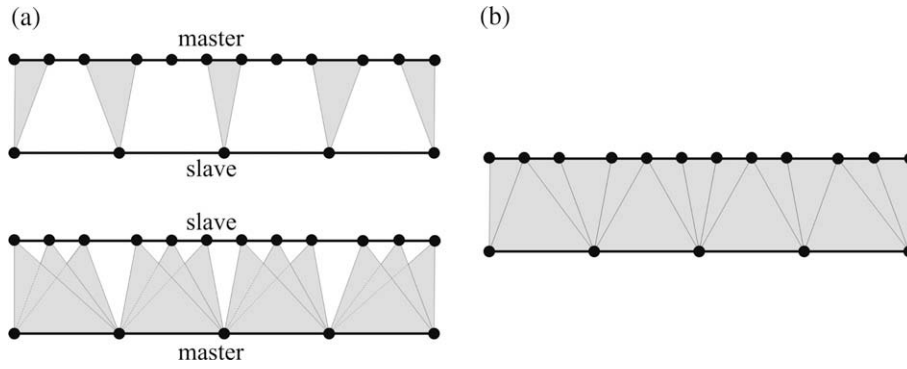


Fig. 2. Contact pairing: (a) node-to-segment and (b) contact domain.

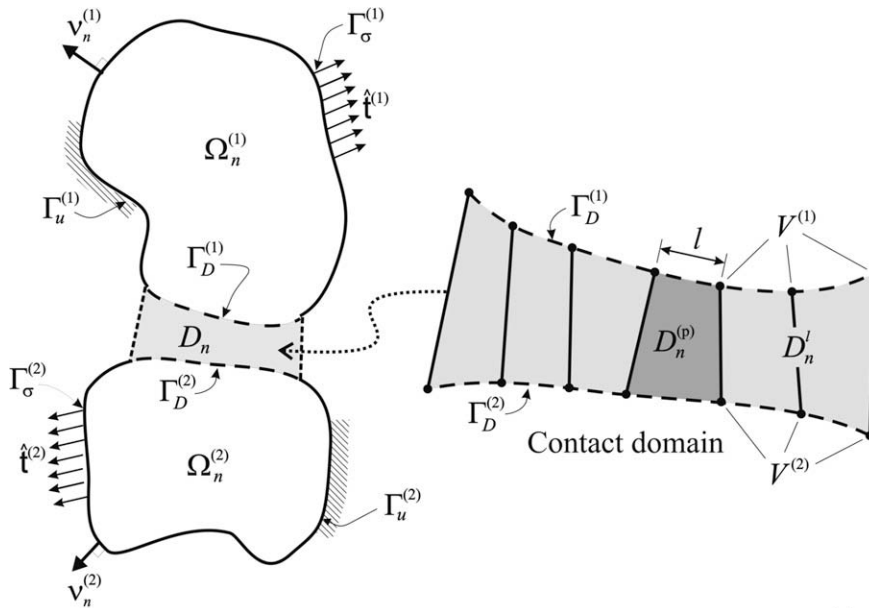


Fig. 3. Definition of the contact domain D_n between two contacting bodies $\Omega^{(x)}$ and its subdivision into patches $D_n^{(p)}$.

considered, which connects the coordinates of a particle in the reference and the current configuration via

$$\mathbf{x}^{(x)} = \phi_t^{(x)}(\mathbf{X}^{(x)}) = \mathbf{X}^{(x)} + \mathbf{U}_t^{(x)}(\mathbf{X}^{(x)}). \quad (1)$$

Assume that the time domain $t \in [0, T]$ is subdivided in discrete intervals with $[t_n, t_{n+1}]$ being the current time increment of length $\Delta t_{n+1} = t_{n+1} - t_n$. Then $\Omega_n^{(x)} = \phi_{t_n}^{(x)}(\mathcal{B}^{(x)}) \equiv \phi_n^{(x)}(\mathcal{B}^{(x)})$ and $\Omega_{n+1}^{(x)} = \phi_{t_{n+1}}^{(x)}(\mathcal{B}^{(x)}) \equiv \phi_{n+1}^{(x)}(\mathcal{B}^{(x)})$ are the configurations at time t_n and t_{n+1} . From now on t_n and t_{n+1} will be termed the *previous* and *current times*, and $\Omega_n^{(x)}$ and $\Omega_{n+1}^{(x)}$ the *previous* and *current configurations*, respectively. Specification of Eq. (1) for t_n and t_{n+1} allows defining:

$$\left. \begin{aligned} \mathbf{x}_{n+1}^{(x)} &= \phi_{n+1}^{(x)}(\mathbf{X}^{(x)}) \\ \mathbf{x}_n^{(x)} &= \phi_n^{(x)}(\mathbf{X}^{(x)}) \end{aligned} \right\} \Rightarrow \mathbf{x}_{n+1}^{(x)} = \phi_{n+1}^{(x)} \left(\left(\phi_n^{(x)} \right)^{-1} \left(\mathbf{x}_n^{(x)} \right) \right) = \phi^{(x)} \left(\mathbf{x}_n^{(x)} \right) \quad \forall \mathbf{x}_n^{(x)} \in \Omega_n^{(x)}, \quad (2)$$

where $\phi^{(x)}$, obtained from elimination of the material coordinates $\mathbf{X}^{(x)}$ in Eq. (2), defines the *incremental motion* of the contacting bodies in the current time interval. From this incremental motion, the *incremental displacement field* can be defined as:

$$\mathbf{u}^{(x)}(\mathbf{x}_n^{(x)}) = \phi^{(x)}(\mathbf{x}_n^{(x)}) - \mathbf{x}_n^{(x)} = \mathbf{x}_{n+1}^{(x)} - \mathbf{x}_n^{(x)} \quad \forall \mathbf{x}_n^{(x)} \in \Omega_n^{(x)}. \quad (3)$$

Let $\partial\Omega_n^{(x)}$ be the boundary of $\Omega_n^{(x)}$ at the previous configuration and $\mathbf{v}_n^{(x)}$ the corresponding outward normal (see Fig. 3). Then, a so-called *contact domain* D_n , with boundary ∂D_n , joining part of the boundaries $\partial\Omega_n^{(x)}$, i.e. $\Gamma_D^{(x)} = \partial\Omega_n^{(x)} \cap \partial D_n$, is defined. Assume that $\Gamma_D^{(x)}$ are large enough to contain those parts of $\partial\Omega_n^{(x)}$ that are coming into contact at the end of the current time interval $[t_n, t_{n+1}]$ (thus at time t_{n+1}).

Assume that there may be a suitable number of vertices $V_i^{(x)}$ conveniently placed in the contacting boundaries $\Gamma_D^{(x)}$ and that, on base of these vertices, the contact domain D_n can be approximated by a domain D_n^l (where superscript l refers to the typical value of the vertices separation) partitioned in n_p patches $D_n^{(p)}$ such that

$$D_n \approx D_n^l = \bigcup_{p=1}^{n_p} D_n^{(p)}. \quad (4)$$

Remark 2-1. Although the vertices $V_i^{(x)}$ might be, in principle, chosen independently of the discretization of the contacting bodies $\mathcal{B}^{(x)}$, in the context of the finite element method the natural choice is that they coincide with the finite element nodes on the contacting boundaries $\Gamma_D^{(x)}$.

This partition has the following properties:

- (a) It consists of a *unique layer of patches*.
- (b) The contact patches $D_n^{(p)}$ do not overlap, and D_n^l converges to the contact domain D_n as the number of vertices increases (or, equivalently, $l \rightarrow 0$).

2.2. Contact patches for two-dimensional problems

Assuming, that the vertices $V_i^{(x)}$ to approximate the contact domain coincide with finite element nodes placed on $\Gamma_D^{(x)}$ (see Remark 2-1), various types of contact patches might be defined. Some possibilities for two-dimensional problems are sketched in Fig. 4.

In principle, a contact patch may have a *quadrilateral* (see Fig. 4a and c) or a *triangular* (see Fig. 4b and d) shape, regardless of the utilized finite element formulation in the contacting bodies (linear, quadratic or higher order elements).

Having in mind the explicit construction of these patches as well as the resulting contact formulation, the triangular linear-linear shaped variant seems to have some advantages:

- (a) The construction of linear triangular shaped patches may be done by means of a simple constrained Delaunay triangulation [10] on basis of the cloud of vertices $V_i^{(x)}$ and the corresponding outward normals $\mathbf{v}^{(x)}$. This method fulfills the requirements stated in Section 2.1 above.
- (b) Anticipating subsequent results (see Section 5.2), the resulting contact formulation within one contact patch will be easier, but this not necessarily meaning a loss of effectiveness.

Due to these considerations, in the main body of this work the authors have chosen linear triangular shaped patches to approximate the contact domain. However, in order to be explored out of this work, specific geometrical definitions for the use of a linear-quadratic triangular contact patch are given in Appendix B.

Remark 2-2. It has to be emphasized that utilizing linear triangular shaped patches for the approximation of the contact domain does not imply any limitation in the type of elements utilized in the discretization of the contacting bodies, which can be triangular or quadrilateral finite elements of any order.

2.3. Linear triangular contact patch

2.3.1. Incremental motion

Although the incremental motion $\phi^{(x)}$ and the incremental displacements $\mathbf{u}^{(x)}$, in Eqs. (2) and (3), are only defined in the domains $\Omega_n^{(x)}$, the contact domain D_n^l is endowed with an extension of this incremental displacement field, $\mathbf{u}^{(D)}$, for the purpose of supplying a mathematical expression to the gap based in classical strain measures (see Section 2.4.1). Thus, the incremental motion $\phi^{(D)}$ of the contact domain D_n^l may be written as

$$\begin{aligned} \phi^{(D)} : D_n^l &\rightarrow D_{n+1}^l, \\ \phi^{(D)}(\mathbf{x}_n) &\equiv \mathbf{x}_{n+1}(\mathbf{x}_n) = \mathbf{x}_n + \mathbf{u}^{(D)}(\mathbf{x}_n) \quad \forall \mathbf{x}_n \in D_n^l, \end{aligned} \tag{5}$$

where the *current contact domain* D_{n+1}^l is the convected one of D_n^l through $\phi^{(D)}$, i.e. $D_{n+1}^l = \phi^{(D)}(D_n^l)$ (see Fig. 5). Also, the contacting domains in the current configuration are $\gamma_D^{(x)} = \phi^{(D)}(\Gamma_D^{(x)})$, $(\alpha = 1, 2)$.

The incremental displacement field $\mathbf{u}^{(D)}$ is linearly interpolated from the corresponding incremental displacements of the boundaries, thus for a linear triangle contact patch it can be specified with

$$\mathbf{u}^{(D)}(\mathbf{x}_n) \equiv \mathbf{u}^{(p)}(\mathbf{x}_n) = \sum_{i=1}^3 N_i(\mathbf{x}_n) \mathbf{d}_i^{(D)} \quad \forall \mathbf{x}_n \in D_n^{(p)}, \tag{6}$$

where N_i are the standard linear interpolation functions for triangular finite elements [33] and $\mathbf{d}_i^{(D)}$ are the *incremental displacements* at the vertices 1, 2, 3 of patch p . Due to the linear format of the incremental motion in Eq. (6), the convected contact domain D_{n+1}^l is also a linear triangulation, approximating the current contact domain D_{n+1} . According to the incremental motion $\phi^{(D)}$ given in Eq. (5), one can now define strain measures of this motion, in particular the *incremental gradient of deformation tensor*:

$$\mathbf{f}^{(D)} = \text{GRAD}(\phi^{(D)}(\mathbf{x}_n)) = \frac{\partial \mathbf{x}_{n+1}}{\partial \mathbf{x}_n} = \mathbf{1} + \text{GRAD}(\mathbf{u}^{(D)}), \tag{7}$$

where $\mathbf{1}$ stands for the second order unit tensor and Eq. (5) has been considered.

Remark 2-3. Notice that, due to the linear character of the incremental displacement field in Eq. (6), $\text{GRAD}(\mathbf{u}^{(D)})$ and $\mathbf{f}^{(D)}$ are *constant within every contact patch*, i.e.:

$$\mathbf{f}^{(D)}(\mathbf{x}_n) \equiv \mathbf{f}^{(p)} = \text{constant} \quad \forall \mathbf{x}_n \in D^{(p)}. \tag{8}$$

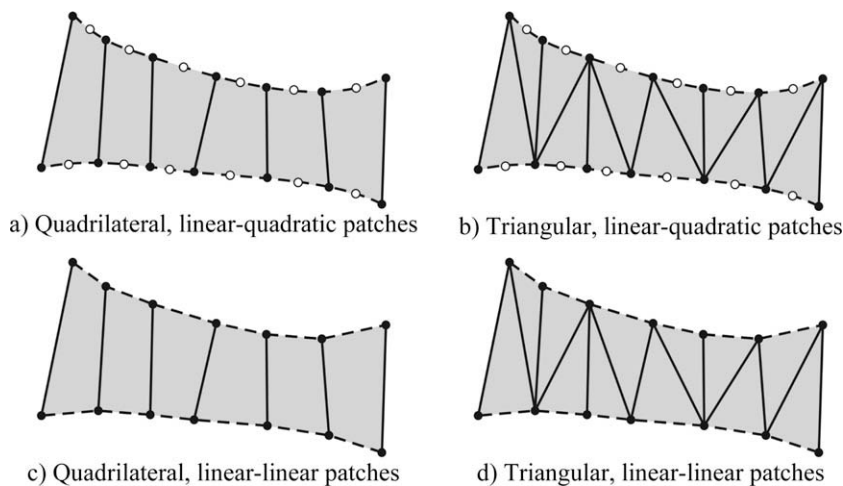


Fig. 4. Possible patch definitions for two-dimensional contact problems.

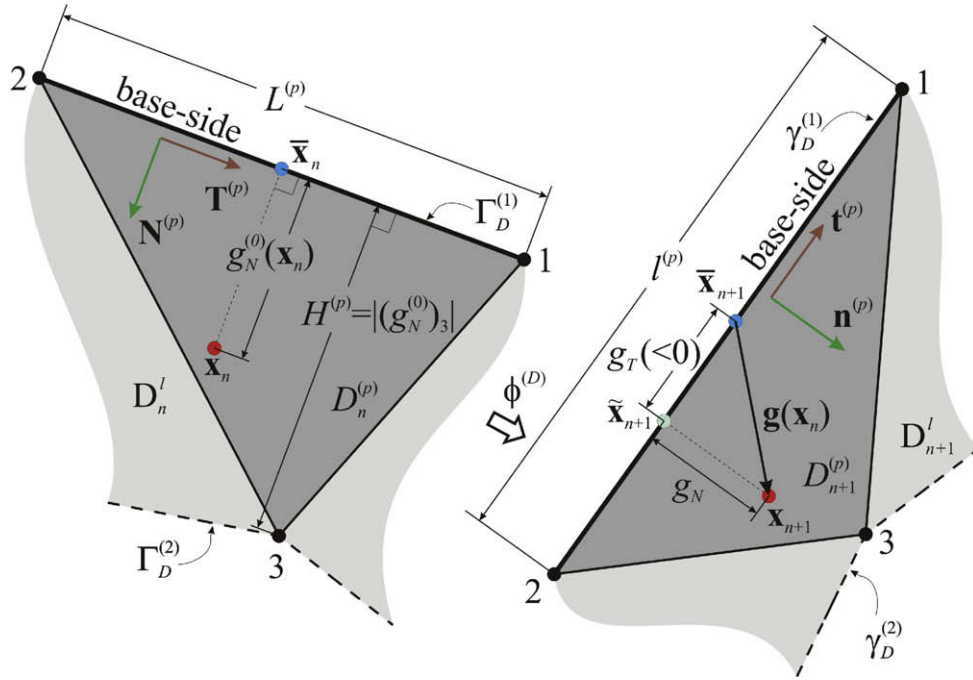


Fig. 5. Linear triangle contact patch in previous and current configuration.

2.3.2. Normal and tangential vectors

Fig. 5 displays a linear triangular contact patch, $D_n^{(p)}$, in the previous configuration. Vector $\mathbf{N}^{(p)}$ is defined as the unit vector normal to the base-side (placed on $\Gamma_D^{(x)}$) in the sense of the corresponding outward normal $\mathbf{v}_n^{(x)}$ of the connected contacting body (i.e. $\mathbf{N}^{(p)} = \mathbf{v}_n^{(x)}$). Accordingly, the tangential vector $\mathbf{T}^{(p)}$ is defined as the anti clockwise unit vector:

$$\mathbf{T}^{(p)} = \hat{\mathbf{e}}_3 \times \mathbf{N}^{(p)}, \quad (9)$$

where $\hat{\mathbf{e}}_3$ stands for the out-of-plane unit vector so that the $\{\mathbf{N}^{(p)}, \mathbf{T}^{(p)}, \hat{\mathbf{e}}_3\}$ is a direct triplet of unit vectors. Considering now the convected patch $D_{n+1}^{(p)} = \phi^{(D)}(D_n^{(p)})$, the current tangent vector $\mathbf{t}^{(p)}$ and the unit normal vector $\mathbf{n}^{(p)}$ are defined, respectively, as the (unit) tangent vector convected from $\mathbf{T}^{(p)}$ and the corresponding orthogonal unit vector:

$$\mathbf{t}^{(p)} = \frac{\phi^{(D)}(\mathbf{T}^{(p)})}{\|\phi^{(D)}(\mathbf{T}^{(p)})\|} = \frac{\mathbf{f}^{(p)} \cdot \mathbf{T}^{(p)}}{\|\mathbf{f}^{(p)} \cdot \mathbf{T}^{(p)}\|}, \quad (10)$$

$$\mathbf{n}^{(p)} = \mathbf{t}^{(p)} \times \hat{\mathbf{e}}_3$$

so that $\{\mathbf{n}^{(p)}, \mathbf{t}^{(p)}, \hat{\mathbf{e}}_3\}$ is also a direct triplet of unit vectors. It can be readily proven that the definition of $\mathbf{n}^{(p)}$ in Eq. (10) preserves its outward character with respect to $\gamma_D^{(x)}$ (i.e. $\mathbf{n}^{(p)} = \mathbf{v}_{n+1}^{(x)}$).

Remark 2-4. Notice, from the procedure for their construction in Eq. (10), that $\mathbf{n}^{(p)}$ and $\mathbf{t}^{(p)}$ are constant in the convected patch $D_{n+1}^{(p)} = \phi^{(D)}(D_n^{(p)})$. However, the definition of the normal and tangential vectors $\mathbf{N}^{(p)}$ and $\mathbf{T}^{(p)}$, is done locally within every contact patch $D_n^{(p)}$ on basis of its base-side (see Fig. 5). Therefore the normal and tangential vector fields $\mathbf{n}^{(p)}$ and $\mathbf{t}^{(p)}$ may be discontinuous from patch to patch within the current contact domain D_{n+1}^l .

2.4. Gap definition

2.4.1. Geometrical gap

Starting from the previous configuration, the *initial normal gap* $g_N^{(0)}$ will be defined for every given point of a contact patch

$\mathbf{x}_n \in D_n^{(p)}$ as the signed distance from its N -projection on the base-side $\bar{\mathbf{x}}_n \in \Gamma_D^{(x)}$ (see Fig. 5), i.e.:

$$g_N^{(0)}(\mathbf{x}_n) = (\mathbf{x}_n - \bar{\mathbf{x}}_n) \cdot \mathbf{N}(\mathbf{x}_n). \quad (11)$$

In the contact patch $D_{n+1}^{(p)}$, at the current contact domain, the *final gap vector* $\mathbf{g}(\mathbf{x}_n)$ is defined with

$$\mathbf{g}(\mathbf{x}_n) = \mathbf{x}_{n+1} - \bar{\mathbf{x}}_{n+1} = \phi^{(D)}(\mathbf{x}_n) - \phi^{(D)}(\bar{\mathbf{x}}_n), \quad (12)$$

where $\mathbf{x}_{n+1} = \phi^{(D)}(\mathbf{x}_n)$ and $\bar{\mathbf{x}}_{n+1} = \phi^{(D)}(\bar{\mathbf{x}}_n)$ are the convected points of \mathbf{x}_n and $\bar{\mathbf{x}}_n$, respectively. The definitions for the normal and tangential gaps (g_N, g_T) can then be given as the projections of the final gap vector $\mathbf{g}(\mathbf{x}_n)$ onto the current normal and tangential directions

$$\mathbf{g}(\mathbf{x}_n) = g_N(\mathbf{x}_n)\mathbf{n}^{(p)} + g_T(\mathbf{x}_n)\mathbf{t}^{(p)} \Rightarrow \begin{cases} g_N(\mathbf{x}_n) = \mathbf{g}(\mathbf{x}_n) \cdot \mathbf{n}^{(p)}, \\ g_T(\mathbf{x}_n) = \mathbf{g}(\mathbf{x}_n) \cdot \mathbf{t}^{(p)}. \end{cases} \quad (13)$$

Remark 2-5. Notice that the definition of the normal gap in Eq. (13) is completely equivalent to the (signed) distance from a point \mathbf{x}_{n+1} to the base-line of the corresponding contact patch $D_{n+1}^{(p)}$. Negative values of g_N indicate penetration of the considered point. The tangential gap g_T can also be identified as the *slid distance* (during the current time step) of the projection of the point on that base-line in the sense of $\mathbf{t}^{(p)}$.

Now, considering the Taylor's expansion:

$$\begin{aligned} \mathbf{x}_{n+1} &= \phi^{(D)}(\mathbf{x}_n) = \phi^{(D)}(\bar{\mathbf{x}}_n + g_N^{(0)}(\mathbf{x}_n)\mathbf{N}^{(p)}) \\ &= \phi^{(D)}(\bar{\mathbf{x}}_n) + \text{GRAD}(\phi^{(D)}) \cdot (g_N^{(0)}(\mathbf{x}_n)\mathbf{N}^{(p)}) \\ &= \bar{\mathbf{x}}_{n+1} + g_N^{(0)}(\mathbf{x}_n)\mathbf{f}^{(p)} \cdot \mathbf{N}^{(p)}, \end{aligned} \quad (14)$$

where higher order terms are exactly zero due to the constant character of $\mathbf{f}^{(p)}$ (see Remark 2-3 and Eq. (8)). Then the final gap vector $\mathbf{g}(\mathbf{x}_n)$ (in Eq. (12)) can be written as

$$\begin{aligned} \mathbf{g}(\mathbf{x}_n) &= \mathbf{x}_{n+1} - \bar{\mathbf{x}}_{n+1} = g_N^{(0)}(\mathbf{x}_n)\mathbf{f}^{(p)} \cdot \mathbf{N}^{(p)} \\ &= g_N^{(0)}(\mathbf{x}_n)(\mathbf{1} + \text{GRAD}(\mathbf{u}^{(p)})) \cdot \mathbf{N}^{(p)} \end{aligned} \quad (15)$$

which leads to the expressions for the normal and tangential gaps in Eq. (13):

$$\begin{aligned} \mathbf{g}_N(\mathbf{x}_n) &= \mathbf{n}^{(p)} \cdot \mathbf{g}(\mathbf{x}_n) = \mathbf{g}_N^{(0)}(\mathbf{x}_n) \mathbf{n}^{(p)} \cdot \mathbf{f}^{(p)} \cdot \mathbf{N}^{(p)} \\ &= \mathbf{g}_N^{(0)}(\mathbf{x}_n) \mathbf{n}^{(p)} \cdot (\mathbf{N}^{(p)} + \text{GRAD}(\mathbf{u}^{(p)}) \cdot \mathbf{N}^{(p)}), \\ \mathbf{g}_T(\mathbf{x}_n) &= \mathbf{t}^{(p)} \cdot \mathbf{g}(\mathbf{x}_n) = \mathbf{g}_T^{(0)}(\mathbf{x}_n) \mathbf{t}^{(p)} \cdot \mathbf{f}^{(p)} \cdot \mathbf{N}^{(p)} \\ &= \mathbf{g}_T^{(0)}(\mathbf{x}_n) \mathbf{t}^{(p)} \cdot (\mathbf{N}^{(p)} + \text{GRAD}(\mathbf{u}^{(p)}) \cdot \mathbf{N}^{(p)}). \end{aligned} \quad (16)$$

Remark 2-6. After some algebraic manipulation, it can be proven that the mathematical expressions of the gaps in Eq. (16) coincide, with the ones in classical node-to-segment formulations [28] if \mathbf{x}_n is considered *the (slave) node*, and the base-side of the triangle is considered *the (master) segment* (see also Section 5.2). However, there are some remarkable differences emerging from Eq. (16):

- The gaps are here defined for all points of the contact patch $D_n^{(p)}$ and not only for the vertices (nodes) in the contacting boundaries $\Gamma_D^{(x)}$. This is going to be exploited for the mathematical and numerical formulation of the contact problem.
- The gaps are defined in terms of strain measures ($\mathbf{f}^{(p)}$, $\text{GRAD}(\mathbf{u}^{(p)})$) of the incremental displacement motion endowed to the contact domain. This makes straightforward the generalization of those expressions to wider contexts to be explored: i.e.: non-triangular partitions of the contact domain, non-linear character of the displacement field in the contact domain (see Appendix B for an example for a quadratic triangular patch), and extensions to 3D cases, where pairing scenarios other than node-to-surface appear in the contact domain method. For instance, when linear tetrahedra are used for partitioning 3D domains, segment-to-segment pairings appear in addition to node-to-surface pairings.

2.4.2. Gap intensities

It can be anticipated that, when using a contact domain method, the basic gap measures appearing in the variational formulation are dimensionless entities (see Section 4). Therefore the dimensionless *gap intensities* \bar{g}_N and \bar{g}_T are introduced, being the values of the current gaps per unit of the initial normal gap:

$$\bar{g}_N(\mathbf{x}_n) = \frac{\mathbf{g}_N(\mathbf{x}_n)}{\left| \mathbf{g}_N^{(0)}(\mathbf{x}_n) \right|} \quad \text{and} \quad \bar{g}_T(\mathbf{x}_n) = \frac{\mathbf{g}_T(\mathbf{x}_n)}{\left| \mathbf{g}_T^{(0)}(\mathbf{x}_n) \right|}. \quad (17)$$

From Eq. (17) the following relations hold:

$$\left. \begin{aligned} \bar{g}_N(\mathbf{x}_n) \geq 0 \Rightarrow \mathbf{g}_N(\mathbf{x}_n) = \left| \mathbf{g}_N^{(0)}(\mathbf{x}_n) \right| \bar{g}_N(\mathbf{x}_n) \geq 0 \\ \text{sign}(\bar{g}_T(\mathbf{x}_n)) = \text{sign}(\mathbf{g}_T(\mathbf{x}_n)) \end{aligned} \right\} \quad \forall \mathbf{x}_n \in D_n^{(p)}. \quad (18)$$

Therefore, imposition of the non-penetration condition in terms of the normal gap intensity ($\bar{g}_N(\mathbf{x}_n) \geq 0$) is equivalent to the imposition of this condition in terms of the normal gap ($\mathbf{g}_N(\mathbf{x}_n) \geq 0$) at all points of a contact patch. In addition, a friction law based on the sign of the tangential gap \mathbf{g}_T , is equivalent to the one in terms of the sign of the tangential gap intensity \bar{g}_T . In summary, imposition of the mechanical contact (friction) conditions is going to be done in terms of the gap intensities \bar{g}_N and \bar{g}_T , being equivalent to its imposition in terms of the geometrical gaps \mathbf{g}_N and \mathbf{g}_T .

Remark 2-7. In view of Eq. (17) one could wonder about the singularity of the gap intensities \bar{g}_N and \bar{g}_T when $\mathbf{g}_N^{(0)}(\mathbf{x}_n) = 0 \quad \forall \mathbf{x}_n \in D_n^{(p)}$ (perfect normal contact in the patch at the previous configuration). Then, \bar{g}_N and \bar{g}_T could become unbounded, this possibly translating into ill conditioning of the formulation. In fact, it can be anticipated that, in the variational formulation of the problem in

Sections 4 and 5, the gap intensities \bar{g}_N and \bar{g}_T appear in integral expressions of the type:

$$\int_{D_n^{(p)}} (\bullet) \bar{g}_N(\mathbf{x}_n) dD; \quad \int_{D_n^{(p)}} (\bullet) \bar{g}_T(\mathbf{x}_n) dD, \quad (19)$$

where (\bullet) are bounded entities. When there is a *perfect normal contact* in the patch at the previous configuration (the triangular patch $D_n^{(p)}$ is perfectly flat) the measure of the integration domain is $\text{meas}(D_n^{(p)}) = 0$. Therefore, the integrals in Eq. (19) have unbounded kernels and a null measure of the integration domain. However, it will be shown (see Remark 5-3 below) that those integrals are convergent to bounded values and, thus, that the unbounded character of the gap intensities \bar{g}_N and \bar{g}_T does not translate into ill conditioning of the problem.

Inserting the geometrical gap definitions in Eq. (16), the gap intensities defined in Eq. (17) can be written as

$$\begin{aligned} \bar{g}_N^{(p)} &= \frac{\mathbf{g}_N(\mathbf{x}_n)}{\left| \mathbf{g}_N^{(0)}(\mathbf{x}_n) \right|} = \text{sign} \left(\mathbf{g}_N^{(0)}(\mathbf{x}_n) \right) \mathbf{n}^{(p)} \cdot (\mathbf{N}^{(p)} + \text{GRAD}(\mathbf{u}^{(p)}) \cdot \mathbf{N}^{(p)}), \\ \bar{g}_T^{(p)} &= \frac{\mathbf{g}_T(\mathbf{x}_n)}{\left| \mathbf{g}_T^{(0)}(\mathbf{x}_n) \right|} = \text{sign} \left(\mathbf{g}_T^{(0)}(\mathbf{x}_n) \right) \mathbf{t}^{(p)} \cdot (\mathbf{N}^{(p)} + \text{GRAD}(\mathbf{u}^{(p)}) \cdot \mathbf{N}^{(p)}) \end{aligned} \quad (20)$$

Remark 2-8. Notice, from Eq. (20), and Remarks 2-3 and 2-4, that $\bar{g}_N^{(p)}$ and $\bar{g}_T^{(p)}$ are constant in every linear triangular patch $D_n^{(p)}$ of the contact domain. This is why, in Eq. (20), superscript $(\bullet)^{(p)}$ identifies the constant entities for the whole contact patch p .

2.4.3. Variations of gap intensities

For subsequent numerical implementation, it is necessary to derive the Gâteaux variations of the gap intensities in Eq. (20). Detailed derivations, based on standard manipulation of strain measures in classical continuum mechanics [6], can be found in Appendix A.1. In the following, a summary of the most relevant expressions is provided. For a more compact writing, the superscript $(\bullet)^{(p)}$ will be omitted.

The variations of the current normal and tangential vectors in Eq. (10) read:

$$\begin{aligned} \delta \mathbf{n} &= -(\mathbf{n} \cdot \text{grad}(\delta \mathbf{u})) \cdot \mathbf{t} = -(\mathbf{t} \otimes \mathbf{n}) \cdot \frac{\partial \delta \mathbf{u}}{\partial \mathbf{t}}, \\ \delta \mathbf{t} &= (\mathbf{n} \cdot \text{grad}(\delta \mathbf{u})) \cdot \mathbf{n} = (\mathbf{n} \otimes \mathbf{n}) \cdot \frac{\partial \delta \mathbf{u}}{\partial \mathbf{t}}, \end{aligned} \quad (21)$$

where $\text{grad}(\bullet) = \frac{\partial(\bullet)}{\partial \mathbf{x}_{n+1}} = \text{GRAD}(\bullet) \cdot \mathbf{f}^{-1}$ stands for the spatial gradient of entity (\bullet) and $\frac{\partial(\bullet)}{\partial \mathbf{t}} = \text{grad}(\bullet) \cdot \mathbf{t}$ is the corresponding spatial t -directional derivative. With the expressions Eq. (21) the variation of the normal and tangential gap intensities in Eq. (20) can be derived as:

$$\begin{aligned} \delta \bar{g}_N &= \bar{g}_N \mathbf{n} \cdot \text{grad}(\delta \mathbf{u}) \cdot \mathbf{n}, \\ \delta \bar{g}_T &= \bar{g}_N (\mathbf{n} \cdot \text{grad}(\delta \mathbf{u})) \cdot \mathbf{t} + \mathbf{t} \cdot \text{grad}(\delta \mathbf{u}) \cdot \mathbf{n} + \bar{g}_T \mathbf{t} \cdot \text{grad}(\delta \mathbf{u}) \cdot \mathbf{t}. \end{aligned} \quad (22)$$

2.4.4. Linearization of the gap intensities and their variations

For the purposes of using them in an implicit Newton-Raphson solution scheme the corresponding linearized expressions, denoted as $\Delta(\bullet)$ and derived in Appendix A.1, are given next:

$$\begin{aligned} \Delta \bar{g}_N &= \bar{g}_N \mathbf{n} \cdot \text{grad}(\Delta \mathbf{u}) \cdot \mathbf{n}, \\ \Delta \bar{g}_T &= \bar{g}_N (\mathbf{n} \cdot \text{grad}(\Delta \mathbf{u})) \cdot \mathbf{t} + \mathbf{t} \cdot \text{grad}(\Delta \mathbf{u}) \cdot \mathbf{n} + \bar{g}_T \mathbf{t} \cdot \text{grad}(\Delta \mathbf{u}) \cdot \mathbf{t}, \end{aligned} \quad (23)$$

$$\Delta\delta\bar{g}_N(\delta\mathbf{u}, \Delta\mathbf{u}) = -\bar{g}_N \left[\left(\mathbf{n} \cdot \frac{\partial\delta\mathbf{u}}{\partial t} \right) \left(\mathbf{n} \cdot \frac{\partial\Delta\mathbf{u}}{\partial t} \right) + \left(\mathbf{n} \cdot \frac{\partial\delta\mathbf{u}}{\partial t} \right) \left(\mathbf{t} \cdot \frac{\partial\Delta\mathbf{u}}{\partial n} \right) + \left(\mathbf{t} \cdot \frac{\partial\delta\mathbf{u}}{\partial n} \right) \left(\mathbf{n} \cdot \frac{\partial\Delta\mathbf{u}}{\partial t} \right) \right], \quad (24)$$

$$\Delta\delta\bar{g}_T(\delta\mathbf{u}, \Delta\mathbf{u}) = \bar{g}_N \left[\left(\mathbf{n} \cdot \frac{\partial\delta\mathbf{u}}{\partial t} \right) \left(\mathbf{n} \cdot \frac{\partial\Delta\mathbf{u}}{\partial n} \right) + \left(\mathbf{n} \cdot \frac{\partial\delta\mathbf{u}}{\partial n} \right) \left(\mathbf{n} \cdot \frac{\partial\Delta\mathbf{u}}{\partial t} \right) \right] - \bar{g}_N \left[\left(\mathbf{t} \cdot \frac{\partial\delta\mathbf{u}}{\partial t} \right) \left(\mathbf{n} \cdot \frac{\partial\Delta\mathbf{u}}{\partial t} \right) + \left(\mathbf{n} \cdot \frac{\partial\delta\mathbf{u}}{\partial t} \right) \left(\mathbf{t} \cdot \frac{\partial\Delta\mathbf{u}}{\partial t} \right) \right] + \bar{g}_T \left(\mathbf{n} \cdot \frac{\partial\delta\mathbf{u}}{\partial t} \right) \left(\mathbf{n} \cdot \frac{\partial\Delta\mathbf{u}}{\partial t} \right). \quad (25)$$

Remark 2-9. Notice the symmetries of the expressions in Eqs. (24) and (25) with respect to variation ($\delta\mathbf{u}$) and linearization ($\Delta\mathbf{u}$), i.e.: $\Delta\delta\bar{g}_N(\delta\mathbf{u}, \Delta\mathbf{u}) = \Delta\delta\bar{g}_N(\Delta\mathbf{u}, \delta\mathbf{u})$.

3. Contact constraints and boundary value problem

The contact restrictions may be split into normal and tangential contact constraints.

3.1. Normal contact constraints

Let $\mathbf{P}^{(\alpha)}(\mathbf{x}_n, t_{n+1})$ denote the first Piola–Kirchhoff stress, at the current time t_{n+1} , measured with respect to the previous ($\Omega_n^{(\alpha)}$) configuration and

$$\mathbf{t}_c(\mathbf{x}_n, \mathbf{N}) = \mathbf{P}^{(\alpha)} \cdot \mathbf{N} \quad \forall \mathbf{x}_n \in \Gamma_D^{(\alpha)} \quad (26)$$

the traction vector acting onto the N -oriented contacting surface $\Gamma_D^{(\alpha)}$ (see Fig. 3) where the normal N is patch-wise defined in the previous contact domain D_n^l (see Fig. 5). Assuming that adhesion is excluded in the contact area, the normal contact traction

$$t_N^{(\alpha)}(\mathbf{x}_n) = \mathbf{n} \cdot \mathbf{t}_c = \mathbf{n} \cdot \mathbf{P}^{(\alpha)} \cdot \mathbf{N} \quad \forall \mathbf{x}_n \in \Gamma_D^{(\alpha)} \quad (27)$$

must be negative ($t_N^{(\alpha)} \leq 0$). In Eq. (27) \mathbf{n} is the patch-wise defined normal in the current contact domain D_{n+1}^l described in Fig. 5.

Additionally the geometrical *impenetrability constraint*

$$\bar{g}_N(\mathbf{x}_n) \geq 0 \quad \forall \mathbf{x}_n \in D_n^l \quad (28)$$

must be satisfied in the contact domain D_n^l . As the normal contact traction $t_N^{(\alpha)}$ only lives on the contacting boundaries $\Gamma_D^{(\alpha)}$, a *normal Lagrange multiplier* $\lambda_N(\mathbf{x}_n) \forall \mathbf{x}_n \in D_n^l$ is introduced, living in the whole previous contact domain and fulfilling

$$\lambda_N(\mathbf{x}_n) = t_N^{(\alpha)}(\mathbf{x}_n) \quad \forall \mathbf{x}_n \in \Gamma_D^{(\alpha)}. \quad (29)$$

Therefore, the normal contact constraints may be summarized in form of the classical *Karush–Kuhn–Tucker* conditions [28], using the introduced normal Lagrange multiplier

$$\lambda_N \leq 0, \quad \bar{g}_N \geq 0, \quad \lambda_N \bar{g}_N = 0 \quad \text{in } D_n^l. \quad (30)$$

3.2. Tangential contact constraints

The formulation of the tangential contact constraints necessitates the definition of an appropriate friction law. In this work, the classical *Coulomb* model is used, which limits the allowable tangential contact stress with

$$\|\mathbf{t}_T\| \leq \mu |t_N|, \quad (31)$$

where μ is the coefficient of friction. The tangential stress \mathbf{t}_T is given by the projection of the traction vector \mathbf{t}_c in Eq. (26) onto the tangent plane, which simplifies for two dimensional problems to

$$t_T^{(\alpha)}(\mathbf{x}_n) = \mathbf{t} \cdot \mathbf{t}_c = \mathbf{t} \cdot \mathbf{P}^{(\alpha)} \cdot \mathbf{N} \quad \forall \mathbf{x}_n \in \Gamma_D^{(\alpha)} \quad (32)$$

with \mathbf{t} being the current unit tangent vector in Fig. 5. As before, a tangential Lagrange multiplier $\lambda_T(\mathbf{x}_n) \forall \mathbf{x}_n \in D_n^l$, fulfilling

$$\lambda_T(\mathbf{x}_n) = t_T^{(\alpha)}(\mathbf{x}_n) \quad \forall \mathbf{x}_n \in \Gamma_D^{(\alpha)} \quad (33)$$

is introduced. To distinguish between the stick and slip state, the slip function

$$\Phi = |\lambda_T| - \mu |\lambda_N| \begin{cases} < 0 \rightarrow \text{stick}, \\ = 0 \rightarrow \text{slip} \end{cases} \quad (34)$$

is defined. In analogy to a plasticity-like formulation, the non-associated slip rule can be written as

$$\bar{g}_T = -\gamma \frac{\lambda_T}{|\lambda_T|} = -\gamma \text{sign}(\lambda_T). \quad (35)$$

Similarly to the normal contact constraints, the tangential contact conditions can then be summarized in form of the *Karush–Kuhn–Tucker* conditions

$$\gamma \geq 0, \quad \Phi \leq 0, \quad \gamma \Phi = 0 \quad \text{in } D_n^l. \quad (36)$$

From this one can extract *the slip constraint*

$$\lambda_T = \mu \text{sign}(\lambda_T) |\lambda_N| = -\mu \text{sign}(\bar{g}_T) |\lambda_N| \quad (37)$$

by using Eq. (34)

$$\Phi = 0 \rightarrow |\lambda_T| - \mu |\lambda_N| = 0 \rightarrow \lambda_T = \mu \text{sign}(\lambda_T) |\lambda_N| \quad (38)$$

and (35)

$$\bar{g}_T = -\gamma \text{sign}(\lambda_T) \rightarrow \text{sign}(\bar{g}_T) = -\text{sign}(\lambda_T) \quad \text{as } \gamma \geq 0 \quad (39)$$

as well as *the stick constraint*

$$\Phi < 0 \rightarrow \gamma = 0 \Rightarrow \bar{g}_T = 0. \quad (40)$$

3.3. Inequality constrained boundary value problem

As the geometrical definitions given in Section 2 are based on the incremental displacements $\mathbf{u}^{(\alpha)}(\mathbf{x}_n^{(\alpha)})$ in Eq. (3), the inequality constrained boundary value problem will be written in a consistent way, taking those displacements as primal unknowns, i.e.:

$$\text{FIND} : \begin{cases} \mathbf{u}^{(\alpha)}(\mathbf{x}_n^{(\alpha)}) : & \Omega_n \rightarrow \mathbb{R}^2, \\ \lambda_N(\mathbf{x}_n) : & D_n \rightarrow \mathbb{R}, \\ \lambda_T(\mathbf{x}_n) : & D_n \rightarrow \mathbb{R}, \end{cases} \quad (41)$$

FULFILLING :

$$\text{Momentum Equation} \quad \rho^{(\alpha)} \ddot{\mathbf{u}}^{(\alpha)} = \text{DIV} \mathbf{P}^{(\alpha)} + \mathbf{b}^{(\alpha)} \quad \text{in } \Omega_n^{(\alpha)}, \quad (42)$$

$$\text{Constitutive model} \quad \mathbf{P}^{(\alpha)} = \Sigma^{(\alpha)}(\mathbf{u}^{(\alpha)}) \quad \text{in } \Omega_n^{(\alpha)}, \quad (43)$$

$$\text{Dirichlet's boundary conditions} \quad \mathbf{u}^{(\alpha)} = \bar{\mathbf{u}}^{(\alpha)} \quad \text{in } \Gamma_u^{(\alpha)}, \quad (44)$$

$$\text{Neumann's boundary conditions} \quad \mathbf{P}^{(\alpha)} \cdot \mathbf{v}^{(\alpha)} = \hat{\mathbf{t}}^{(\alpha)} \quad \text{in } \Gamma_\sigma^{(\alpha)}, \quad (45)$$

$$\text{Lagrange multiplier identification} \quad \left. \begin{matrix} \lambda_N = t_N^{(\alpha)} \\ \lambda_T = t_T^{(\alpha)} \end{matrix} \right\} \quad \text{in } \Gamma_D^{(\alpha)}, \quad (46)$$

Normal contact constraints

$$\lambda_N \leq 0, \quad \bar{g}_N(\mathbf{u}^{(D)}) \geq 0, \quad \lambda_N \bar{g}_N(\mathbf{u}^{(D)}) = 0 \quad \text{in } D_n, \quad (47)$$

Tangential contact constraints

$$\gamma \geq 0, \quad \Phi \leq 0, \quad \gamma \Phi = 0 \quad \text{in } D_n. \quad (48)$$

Herein $\mathbf{P}^{(\alpha)}$ and $\mathbf{b}^{(\alpha)}$ are the first Piola–Kirchhoff stress tensor (measured at the previous configuration $\Omega_n^{(\alpha)}$) and given via an appropriate constitutive relation in Eq. (43)), and the body forces on $\Omega^{(\alpha)}$, respectively. Furthermore, $\ddot{\mathbf{u}}^{(\alpha)}$ and $\rho^{(\alpha)}$ represent, respectively, the material acceleration field and the density of bodies $\mathcal{B}^{(\alpha)}$. The appropriate boundary conditions are given by the prescribed

displacements $\hat{\mathbf{u}}^{(z)}$ and tractions $\hat{\mathbf{t}}^{(z)}$, acting on the correlated boundaries $\Gamma_u^{(z)}$ and $\Gamma_\sigma^{(z)}$. The gap expression $\bar{\mathbf{g}}_N(\mathbf{u}^{(D)})$ in Eq. (47), is the one in Eq. (20)₁. Then, the incremental displacements at the contact domain $\mathbf{u}^{(D)} \equiv \mathbf{u}^{(p)}$, are explicitly defined via Eq. (6), in terms of the incremental displacements at the vertices of the triangulation, $\mathbf{d}_i^{(D)}(\mathbf{u}^{(z)})$, which, in turn, are implicitly defined in terms of the primal unknowns $\mathbf{u}^{(z)}(\mathbf{x}_n)$.

Remark 3-1. The boundary value problem (BVP) given in Eqs. (41)–(48) is written in an *incremental manner*, which means, that the *previous* configuration is taken to be the reference configuration. For example the first Piola–Kirchhoff stress tensor $\mathbf{P}^{(z)}$ is not based on the initial, undeformed configuration but on the *previous* one. However, one could have written the motion for the deformable bodies in the classical total *Lagrangian manner* as well (taking the initial configuration as the reference one) and restrict the incremental setting to the contact part of the problem. Nevertheless, for the sake of clearness and simplicity in the explanation, the authors have decided to write the whole boundary value problem in that incremental manner.

3.4. Equality constrained boundary value problem

In the context of large deformation frictional contact problems the size and position of the contact interface may change permanently. Therefore an active set strategy is utilized to identify the present contact area, as well as the distinction between stick and slip on basis of the normal and tangential Karush–Kuhn–Tucker conditions given in Eqs. (47) and (48).

Hence it will be assumed that both the domains $D_n^{(N)}$ (active normal contact domain) and $D_n^{(T)}$ (active stick domain) are known (or predicted) *in advance* (see Fig. 6) as a result of an active set strategy (described in Section 5) based on the following criteria:

$$D_n^{(N)} := \{\mathbf{x}_n | \lambda_N(\mathbf{x}_n) < 0\} \tag{49}$$

for the active normal contact domain, and

$$D_n^{(T)} := \{\mathbf{x}_n | \Phi(\mathbf{x}_n) < 0\} \tag{50}$$

for the active tangential stick domain, which, in view of the equalities $\lambda_N \bar{\mathbf{g}}_N = 0$ and $\gamma \Phi = 0$ in Eqs. (47) and (48), imply:

$$\begin{aligned} \bar{\mathbf{g}}_N(\mathbf{x}_n) &= 0 \quad \forall \mathbf{x}_n \in D_n^{(N)}, \\ \gamma(\mathbf{x}_n) &= 0 \quad \forall \mathbf{x}_n \in D_n^{(T)} \Rightarrow \bar{\mathbf{g}}_T(\mathbf{x}_n) = 0 \quad \forall \mathbf{x}_n \in D_n^{(T)}, \end{aligned} \tag{51}$$

where Eq. (35) has been considered. Definitions of the active domains in Eqs. (49) and (50) provide the following trivial solutions for λ_N and λ_T in the complementary domains $D_n \setminus D_n^{(N)}$ and $D_n \setminus D_n^{(T)}$:

$$\left. \begin{aligned} \lambda_N(\mathbf{x}_n) &\leq 0 \quad \forall \mathbf{x}_n \in D_n \\ \lambda_N(\mathbf{x}_n) &< 0 \quad \forall \mathbf{x}_n \in D_n^{(N)} \end{aligned} \right\} \Rightarrow \lambda_N(\mathbf{x}_n) = 0 \quad \forall \mathbf{x}_n \in D_n \setminus D_n^{(N)} \tag{52}$$

and

$$\left. \begin{aligned} \Phi(\mathbf{x}_n) &\leq 0 \quad \forall \mathbf{x}_n \in D_n \\ \Phi(\mathbf{x}_n) &< 0 \quad \forall \mathbf{x}_n \in D_n^{(T)} \end{aligned} \right\} \Rightarrow \Phi(\mathbf{x}_n) = 0 \quad \forall \mathbf{x}_n \in D_n \setminus D_n^{(T)}. \tag{53}$$

In addition, in Appendix C the proposition $D_n^{(T)} \subset D_n^{(N)}$ is proven. Then, Eq. (53) with Eqs. (38) and (39) gives:

$$\mathcal{F} \equiv \lambda_T = -\mu \text{sign}(\bar{\mathbf{g}}_T) |\lambda_N| \quad \forall \mathbf{x}_n \in D_n \setminus D_n^{(T)}. \tag{54}$$

Eqs. (52) and (54) provide closed form solutions for the Lagrange multipliers λ_N and λ_T at the complementary domains $D_n \setminus D_n^{(N)}$ and $D_n \setminus D_n^{(T)}$, respectively. Therefore, these domains can be excluded from the domains where these unknowns live in Eq. (41), which now read:

$$\text{FIND : } \begin{cases} \mathbf{u}^{(z)}(\mathbf{x}_n^{(z)}) : \Omega_n \rightarrow \mathbb{R}^2 \\ \lambda_N(\mathbf{x}_n) : D_n^{(N)} \rightarrow \mathbb{R}^-, \\ \lambda_T(\mathbf{x}_n) : D_n^{(T)} \rightarrow \mathbb{R}. \end{cases} \tag{55}$$

Additionally, Eqs. (47) and (48) of the original problem now change to:

Coulomb’s friction law

$$\mathcal{F} \equiv \lambda_T = -\mu \text{sign}(\bar{\mathbf{g}}_T) |\lambda_N| \text{ in } D_n^{(N)} \setminus D_n^{(T)}, \tag{56}$$

Constraint conditions

$$\begin{aligned} \bar{\mathbf{g}}_N &= \mathbf{0} \quad \text{in } D_n^{(N)}, \\ \bar{\mathbf{g}}_T &= \mathbf{0} \quad \text{in } D_n^{(T)}, \end{aligned} \tag{57}$$

where now Eq. (57) are equality constraints in terms of the normal and the tangential gap intensities $\bar{\mathbf{g}}_N$ and $\bar{\mathbf{g}}_T$, respectively.

4. Weak form of the frictional contact problem

As a mathematical basis for the numerical solution of the equality constrained boundary value problem given in Section 3.4 (defined by Eqs. (55), (42), (43), (44), (45), (46), (56) and (57)), a weak form of the frictional, large deformation contact problem is introduced. It basically consists of two parts, namely the virtual work principle and the variational constraint equations.

4.1. Virtual work principle

To state the virtual work, first solution and weighting spaces \mathcal{V} and \mathcal{V}_0 are defined, consisting of solutions \mathbf{u} and their variations $\delta \mathbf{u}$ according to

$$\mathcal{V} := \{\mathbf{u}^{(z)} \in H^1(\Omega^{(z)}), \quad \mathbf{u}^{(z)} = \hat{\mathbf{u}}^{(z)} \text{ on } \Gamma_u^{(z)}\} \tag{58}$$

and

$$\mathcal{V}_0 := \{\delta \mathbf{u}^{(z)} \in H^1(\Omega^{(z)}), \quad \delta \mathbf{u}^{(z)} = \mathbf{0} \text{ on } \Gamma_u^{(z)}\}, \tag{59}$$

where $H^1(\Omega^{(z)})$ represents the Sobolev space of functions which have square integrable derivatives. Furthermore the Lagrange multiplier spaces \mathcal{L}_N and \mathcal{L}_T are introduced with

$$\mathcal{L}_N := \{\mu_N : D \rightarrow \mathbb{R}^- | \mu_N \in L^2(D)\} \tag{60}$$

and

$$\mathcal{L}_T := \{\mu_T : D \rightarrow \mathbb{R} | \mu_T \in L^2(D)\}, \tag{61}$$

where $L^2(D)$ represents the Lebesgue space of square integrable functions. Given these spaces, the virtual work principle for the large deformation, frictional contact problem can be written as:

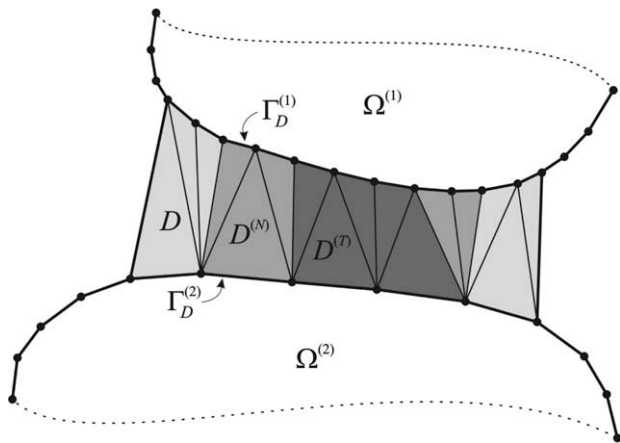


Fig. 6. Active normal and stick domain.

FIND : $\mathbf{u}^{(\alpha)} \in \mathcal{V}$ and $\lambda = [\lambda_N, \lambda_T] \in \mathcal{L}_N \times \mathcal{L}_T$, (62)

FULFILLING :

$$\delta\Pi_{mech}(\mathbf{u}, \lambda, \delta\mathbf{u}) := \delta\Pi_{int,ext}(\mathbf{u}^{(\alpha)}, \delta\mathbf{u}^{(\alpha)}) + \delta\Pi_{cont}(\mathbf{u}^{(\alpha)}, \lambda, \delta\mathbf{u}^{(\alpha)}) = 0$$

$$\forall \delta\mathbf{u}^{(\alpha)} \in \mathcal{V}_0, \quad (63)$$

where $\delta\Pi_{mech}$ stands for the variation of the total mechanical work. In Eq. (63) $\delta\Pi_{int,ext}(\mathbf{u}^{(\alpha)}, \delta\mathbf{u}^{(\alpha)})$ is the sum of the internal and external virtual work done by the two contacting bodies

$$\delta\Pi_{int,ext}(\mathbf{u}^{(\alpha)}, \delta\mathbf{u}^{(\alpha)}) = \delta\Pi_{int}(\mathbf{u}^{(\alpha)}, \delta\mathbf{u}^{(\alpha)}) - \delta\Pi_{ext}(\delta\mathbf{u}^{(\alpha)}) \quad (64)$$

with

$$\delta\Pi_{int}(\mathbf{u}^{(\alpha)}, \delta\mathbf{u}^{(\alpha)}) = \sum_{\alpha=1}^2 \left\{ \int_{\Omega_n^{(\alpha)}} (\rho^{(\alpha)} \ddot{\mathbf{u}}^{(\alpha)} \cdot \delta\mathbf{u}^{(\alpha)} + \mathbf{P}^{(\alpha)} : \text{GRAD}(\delta\mathbf{u}^{(\alpha)})) d\Omega \right\} \quad (65)$$

and

$$\delta\Pi_{ext}(\delta\mathbf{u}^{(\alpha)}) = \sum_{\alpha=1}^2 \left\{ \int_{\Omega_n^{(\alpha)}} \mathbf{b}^{(\alpha)} \cdot \delta\mathbf{u}^{(\alpha)} d\Omega + \int_{\Gamma_\sigma^{(\alpha)}} \hat{\mathbf{t}}^{(\alpha)} \cdot \delta\mathbf{u}^{(\alpha)} d\Gamma \right\} \quad (66)$$

while $\delta\Pi_{cont}(\mathbf{u}^{(\alpha)}, \lambda, \delta\mathbf{u}^{(\alpha)})$ denotes the contact virtual work of the Lagrange multipliers along the variation of the gap intensities in normal and tangential directions, given with

$$\delta\Pi_{cont}(\mathbf{u}^{(\alpha)}, \lambda, \delta\mathbf{u}^{(\alpha)}) = \underbrace{\int_{D_n^{(N)}} \lambda_N \delta\bar{g}_N(\mathbf{u}^D) dD}_{\text{normal contact}} + \underbrace{\int_{D_n^{(T)}} \lambda_T \delta\bar{g}_T(\mathbf{u}^D) dD}_{\text{stick}} + \underbrace{\int_{D_n^{(N)} \setminus D_n^{(T)}} \mathcal{T} \delta\bar{g}_T(\mathbf{u}^D) dD}_{\text{slip}}. \quad (67)$$

As it can be seen in Eq. (67), the contact virtual work expression consists of three different portions defined by integrals over the *active normal contact domain* $D_n^{(N)}$, the *active stick domain* $D_n^{(T)}$ and the *slip domain* $D_n^{(N)} \setminus D_n^{(T)}$.

4.2. Constraint variational equations

The solution of the virtual work expression given in Eq. (63) is constrained by two additional variational equations, stemming from the contact constraints given in Eq. (57), namely

$$\delta\Pi_{\lambda_N}(\mathbf{u}^{(D)}, \delta\lambda_N) = \int_{D_n^{(N)}} \delta\lambda_N \bar{g}_N(\mathbf{u}^{(D)}) dD = 0 \quad \forall \delta\lambda_N \in \mathcal{L}_N \quad (68)$$

and

$$\delta\Pi_{\lambda_T}(\mathbf{u}^{(D)}, \delta\lambda_T) = \int_{D_n^{(T)}} \delta\lambda_T \bar{g}_T(\mathbf{u}^{(D)}) dD = 0 \quad \forall \delta\lambda_T \in \mathcal{L}_T. \quad (69)$$

Remark 4-1. It can be proven that:

- Eqs. (42), (43), (44), (45), (46) and (56) are the Euler–Lagrange equations of the virtual work principle (63).
- Eq. (57) are the Euler–Lagrange equations of the constraint variational Eqs. (68) and (69)

and, therefore, the variational Eqs. (67)–(69) are the weak form of the equality constrained B.V.P. of Section 3.4.

4.3. Discretization

A detailed specification of the spatial discretization of the contacting bodies is not aimed at this point. Indeed, various finite ele-

ment formulations given in the literature may be employed. So that, consider a Galerkin-based discretization: a matrix formulation of the internal and external virtual work done by the contacting bodies (see Eq. (64)) may be stated with the *internal–external residual forces vector* $\mathbf{G}_{int,ext}(\mathbf{d})$ emerging from the virtual work of the internal and external forces:

$$\delta\Pi_{int,ext}(\mathbf{u}, \delta\mathbf{u}) \approx \delta\Pi_{int,ext}^h(\mathbf{d}, \delta\mathbf{d}) \rightarrow \mathbf{G}_{int,ext}(\mathbf{d}) = \sum_{\alpha=1}^2 \left\{ \mathbf{M}^{(\alpha)} \ddot{\mathbf{d}}^{(\alpha)} + \mathbf{F}_{int}^{(\alpha)}(\mathbf{d}^{(\alpha)}) - \mathbf{F}_{ext}^{(\alpha)} \right\}, \quad (70)$$

where $\mathbf{M}^{(\alpha)}$ is the mass matrix, $\mathbf{F}_{int}^{(\alpha)}(\mathbf{d}^{(\alpha)})$ is the vector of deformation dependent internal forces, $\mathbf{F}_{ext}^{(\alpha)}$ is the vector of external forces and $\mathbf{d}^{(\alpha)}$ and $\ddot{\mathbf{d}}^{(\alpha)}$ represent the discrete nodal displacements and accelerations of body α , respectively, and $\mathbf{d} = \{\mathbf{d}^{(1)}, \mathbf{d}^{(2)}\}$ stands for the total set of nodal displacements.

The discretization of the contact virtual work Eq. (67) and the variational constraint Eqs. (68) and (69), necessitates the consideration of interpolations for the Lagrange multipliers, and the displacement field endowed to the contact domain, as well as for their variations, i.e.:

$$\mathbf{u}^{(D)}(\mathbf{x}_n, \mathbf{d}) = \sum N_i(\mathbf{x}_n) \mathbf{d}_i^{(D)} \quad \forall \mathbf{x}_n \in D_n, \quad (71)$$

$$\delta\mathbf{u}^{(D)}(\mathbf{x}_n, \delta\mathbf{d}) = \sum N_i(\mathbf{x}_n) \delta\mathbf{d}_i^{(D)} \quad \forall \mathbf{x}_n \in D_n$$

and

$$\lambda_{N/T}(\mathbf{x}_n, \Lambda) = \sum_j \psi_j(\mathbf{x}_n) \Lambda_{N/T_j} \quad \forall \mathbf{x}_n \in D_n, \quad (72)$$

$$\delta\lambda_{N/T}(\mathbf{x}_n, \delta\Lambda) = \sum_j \psi_j(\mathbf{x}_n) \delta\Lambda_{N/T_j} \quad \forall \mathbf{x}_n \in D_n.$$

Then, the discretization of the contact virtual work expression (67) leads to the *contact residual forces vector* $\mathbf{G}_{cont}(\mathbf{d}, \Lambda)$:

$$\delta\Pi_{cont}(\mathbf{u}, \lambda, \delta\mathbf{u}) \approx \delta\Pi_{cont}^h(\mathbf{d}, \Lambda, \delta\mathbf{d}) \rightarrow \mathbf{G}_{cont}(\mathbf{d}, \Lambda) \quad (73)$$

which depends upon the discrete nodal displacements \mathbf{d} and the discrete values of the Lagrange multipliers Λ . Then, the virtual work principle (63) leads to the *mechanical residual forces*:

$$\delta\Pi_{mech}(\mathbf{u}, \lambda, \delta\mathbf{u}) \approx \delta\Pi_{mech}^h(\mathbf{d}, \lambda, \delta\mathbf{d}) \rightarrow \mathbf{G}_{mech}(\mathbf{d}, \Lambda) = \mathbf{G}_{int,ext}(\mathbf{d}) + \mathbf{G}_{cont}(\mathbf{d}, \Lambda). \quad (74)$$

Furthermore, the discretization of the constraint Eqs. (68) and (69) leads to following *constraint residual vectors*:

$$\delta\Pi_{\lambda_N}(\mathbf{u}^{(D)}, \delta\lambda_N) \approx \delta\Pi_{\lambda_N}^h(\mathbf{d}, \delta\Lambda) = 0 \quad \forall \delta\Lambda_N \rightarrow \mathbf{C}_N(\mathbf{d}) = 0 \quad (75)$$

and

$$\delta\Pi_{\lambda_T}(\mathbf{u}^{(D)}, \delta\lambda_T) \approx \delta\Pi_{\lambda_T}^h(\mathbf{d}, \delta\Lambda) = 0 \quad \forall \delta\Lambda_T \rightarrow \mathbf{C}_T(\mathbf{d}) = 0. \quad (76)$$

The specification of the residual vectors \mathbf{G}_{mech} , \mathbf{C}_N and \mathbf{C}_T will not be detailed here, as the authors only want to emphasize the dependencies of these quantities on the problem unknowns. With these vectors at hand, the discretized problem to be solved can be expressed in terms of the discrete nodal displacements \mathbf{d} and the discrete values of the Lagrange multipliers Λ as:

FIND \mathbf{d} and Λ FULFILLING :

$$\mathbf{G}_{mech}(\mathbf{d}, \Lambda) := \mathbf{G}_{int,ext}(\mathbf{d}) + \mathbf{G}_{cont}(\mathbf{d}, \Lambda) = 0, \quad (77)$$

$$\mathbf{G}_{const}(\mathbf{d}) := \left\{ \begin{matrix} \mathbf{C}_N(\mathbf{d}), \\ \mathbf{C}_T(\mathbf{d}). \end{matrix} \right\} = 0$$

This system of non-linear equations may be solved iteratively using a Newton–Raphson method, which necessitates the linearization of Eq. (77) as:

$$\begin{bmatrix} \mathbf{G}_{mech}(\mathbf{d}, \Lambda) \\ \mathbf{G}_{const}(\mathbf{d}) \end{bmatrix} + \begin{bmatrix} \frac{\partial \mathbf{G}_{mech}(\mathbf{d}, \Lambda)}{\partial \mathbf{d}} & \frac{\partial \mathbf{G}_{mech}(\mathbf{d}, \Lambda)}{\partial \Lambda} \\ \frac{\partial \mathbf{G}_{const}(\mathbf{d})}{\partial \mathbf{d}} & \mathbf{0} \end{bmatrix} \begin{bmatrix} \Delta \mathbf{d} \\ \Delta \Lambda \end{bmatrix} = \begin{bmatrix} \mathbf{0} \\ \mathbf{0} \end{bmatrix}. \quad (78)$$

Remark 4-2. Typically, for Lagrange multiplier formulations, zeros appear on the diagonal of the stiffness matrix, which precludes the direct elimination of the Lagrange multipliers. This translates into high computational solution costs, since the extended system is large and sparse, and the number of discrete Lagrange multipliers may change permanently from time step to time step according to the active contact set. Most importantly: the problem can be prone to exhibit locking or instabilities if the BBL condition [33] is not fulfilled by the used discretizations.

4.4. Lambda-solvability. Stabilization

In order to circumvent the problems described in Remark 4-2 a procedure that can be inserted in the context of the *Nitsche method* [19] or the *interior penalty methods* [1,14,18] is proposed. This procedure can be considered as a generalization of the stabilization method presented in [14] for the linear kinematics case. The basic idea is to add stabilization terms to the variational constraint Eqs. (68) and (69), such that their discretized counterparts (\mathbf{C}_N and \mathbf{C}_T in Eqs. (75) and (76)) display a dependency upon the discrete values of the Lagrange multipliers Λ . The motivation of the method is Eq. (46):

$$\left. \begin{array}{l} \lambda_N = t_N^{(x)} \\ \lambda_T = t_T^{(x)} \end{array} \right\} \text{ in } \Gamma_D^{(x)} \quad (79)$$

which is one of the Euler–Lagrange equations emerging from the virtual work principle in Eq. (63). Then, Eqs. (79) are added in weak form into the variational constraint Eqs. (68) and (69), leading to

$$\begin{aligned} \delta \Pi_{\lambda_N}(\mathbf{u}, \lambda_N, \delta \lambda_N) &= \int_{D_n^{(N)}} \delta \lambda_N \bar{g}_N(\mathbf{u}^{(D)}) dD \\ &+ \underbrace{\int_{\partial D_n^{(N)} \cap \Gamma_D^{(x)}} \delta \lambda_N \tau(t_N(\mathbf{u}^{(x)}) - \lambda_N) d\Gamma}_{\text{additional term}} = 0 \quad \forall \delta \lambda_N \in \mathcal{L}_N \end{aligned} \quad (80)$$

and

$$\begin{aligned} \delta \Pi_{\lambda_T}(\mathbf{u}, \lambda_T, \delta \lambda_T) &= \int_{D_n^{(T)}} \delta \lambda_T \bar{g}_T(\mathbf{u}^{(D)}) dD \\ &+ \underbrace{\int_{\partial D_n^{(T)} \cap \Gamma_D^{(x)}} \delta \lambda_T \tau(t_T(\mathbf{u}^{(x)}) - \lambda_T) d\Gamma}_{\text{additional term}} = 0 \quad \forall \delta \lambda_T \in \mathcal{L}_T. \end{aligned} \quad (81)$$

Herein, $\tau > 0$ is a suitable parameter introduced in order to adjust the dimension of the additional term. This modification now leads to constraint residual vectors \mathbf{C}_N and \mathbf{C}_T , that depend on both sets of variables (\mathbf{d}, Λ) . Thus, the linearized system of Eq. (78) changes to

$$\begin{bmatrix} \mathbf{K}_{dd} & \mathbf{K}_{d\Lambda} \\ \mathbf{K}_{Ad} & \mathbf{K}_{AA} \end{bmatrix} \begin{bmatrix} \Delta \mathbf{d} \\ \Delta \Lambda \end{bmatrix} = - \begin{bmatrix} \mathbf{G}_{mech}(\mathbf{d}, \Lambda) \\ \mathbf{G}_{const}(\mathbf{d}, \Lambda) \end{bmatrix} \quad (82)$$

with a full Hessian (stiffness matrix)

$$\begin{bmatrix} \mathbf{K}_{dd} & \mathbf{K}_{d\Lambda} \\ \mathbf{K}_{Ad} & \mathbf{K}_{AA} \end{bmatrix} = \begin{bmatrix} \frac{\partial \mathbf{G}_{mech}(\mathbf{d}, \Lambda)}{\partial \mathbf{d}} & \frac{\partial \mathbf{G}_{mech}(\mathbf{d}, \Lambda)}{\partial \Lambda} \\ \frac{\partial \mathbf{G}_{const}(\mathbf{d}, \Lambda)}{\partial \mathbf{d}} & \frac{\partial \mathbf{G}_{const}(\mathbf{d}, \Lambda)}{\partial \Lambda} \end{bmatrix} \quad (83)$$

that allows for the condensation of the Lagrange multipliers. The final system of equations to solve within one Newton iteration then reads:

$$\mathbf{K}_T^* \Delta \mathbf{d} = -\mathbf{G}^* \quad (84)$$

with

$$\mathbf{K}_T^* = \mathbf{K}_{dd} - \mathbf{K}_{d\Lambda} \mathbf{K}_{AA}^{-1} \mathbf{K}_{Ad} \quad (85)$$

and

$$\mathbf{G}^* = \mathbf{G}_{mech} - \mathbf{K}_{d\Lambda} \mathbf{K}_{AA}^{-1} \mathbf{G}_{const}. \quad (86)$$

Finally, the Lagrange multipliers can then be *condensed out* as with

$$\Delta \Lambda = -\mathbf{K}_{AA}^{-1} (\mathbf{G}_{const} + \mathbf{K}_{Ad} \Delta \mathbf{d}). \quad (87)$$

Remark 4-3. The role of τ could be also regarded as that of a penalty factor, penalizing the terms $(t_N(\mathbf{u}^{(x)}) - \lambda_N)$ and $(t_T(\mathbf{u}^{(x)}) - \lambda_T)$ in Eqs. (80) and (81). This motivates the character of interior *penalty* method of the proposed procedure. However, since that penalized term is part of the Euler–Lagrange equations of the variational principle (63), mesh refinement will automatically force the penalized term to tend to zero. Therefore, the procedure could be qualified as a *consistent penalty method*, and, unlike in non-consistent penalty methods, the penalty factor τ can be made small (or even very small) without affecting, necessarily, the quality of the obtained results.

Remark 4-4. The introduction of stabilization terms only in the constrained variational Eqs. (80) and (81) will result in a matrix system that is not symmetric. Although Heintz and Hansbo [14] have as well proposed a consistent symmetric version of stabilization, the authors have decided to use the stabilization only in the constrained equations, as the Coulomb's friction law makes the problem non-symmetric anyway. Further investigations will be made to explore the benefits arising from a symmetric stabilization procedure.

Remark 4-5. As the stabilization terms in Eqs. (80) and (81) necessitate the stress field at the boundary of the contacting bodies in terms t_N and t_T (see also Eqs. (27) and (32)), the resulting contact stiffness contributions will involve degrees of freedom of finite element nodes not lying on the contact boundaries $\Gamma_D^{(x)}$, which will slightly increase the bandwidth of the resulting matrices. Furthermore, the stress field in the bodies depends upon the constitutive law utilized in the solids. This has to be taken into account carefully when implementing the proposed stabilization method.

5. Active set strategy

The frictional, large deformation problem described in Section 3.4 displays an equality-constraint problem, assuming that the domains $D_n^{(N)}$ and $D_n^{(T)}$, defined in Eqs. (49) and (50), are known in advance. In this section, a specific methodology to determine those domains at the current time step, based on an active set strategy, is presented.

5.1. Discretization

To solve the aforementioned problem in the variational Eqs. (63), (80) and (81) the deformable bodies $\Omega^{(x)}$ are considered discretized using Galerkin-based finite elements, the type and the order of these elements being irrelevant (see also Remark 2-2). Furthermore, the incremental displacement field $\mathbf{u}^{(D)}$ in the contact domain D_n is approximated on basis of the contact patches as indicated in Eq. (6).

Now, the Lagrange multipliers λ_N and λ_T are specified as *patch-wise constant* in terms of appropriated interpolation functions $\psi^{(p)}$. This reads:

$$\lambda_N \approx \lambda_N^h = \sum_{p=1}^{n_N} \psi^{(p)} A_N^{(p)}; \quad \lambda_T \approx \lambda_T^h = \sum_{p=1}^{n_T} \psi^{(p)} A_T^{(p)},$$

$$\psi^{(p)}(\mathbf{x}_n) = \begin{cases} 1 & \forall \mathbf{x}_n \in D^{(p)}, \\ 0 & \forall \mathbf{x}_n \notin D^{(p)}. \end{cases} \quad (88)$$

where n_N and n_T stand, respectively, for the number of patches of $D_n^{(N)}$ and $D_n^{(T)}$.

5.2. Numerical gaps

As it was shown in Section 2.3 (see also Remark 2-3), the usage of linear triangular contact patches leads to patch-wise constant normal and tangential vectors ($\mathbf{n}^{(p)}, \mathbf{t}^{(p)}$) and gap intensities ($\bar{\mathbf{g}}_N^{(p)}, \bar{\mathbf{g}}_T^{(p)}$). Together with the local support of the interpolation functions $\psi^{(p)}(\mathbf{x}_n)$ given in Eq. (88), this allows a decoupled, patch-by-patch solution of the modified variational constraint Eqs. (80) and (81), i.e.:

$$\delta \Pi_{\lambda_N^{(p)}}^h(\mathbf{d}, A_N^{(p)}, \delta A_N^{(p)}) \equiv \int_{D^{(p)}} \delta A_N^{(p)} \bar{\mathbf{g}}_N^{(p)}(\mathbf{d}^{(D)}) dD$$

$$+ \int_{\Gamma_D^{(p)}} \delta A_N^{(p)} \tau^{(p)} (t_N(\mathbf{d}^{(z)}) - A_N^{(p)}) d\Gamma = 0$$

$$\forall \delta A_N^{(p)} \quad p \in \{1, \dots, n_N\} \quad (89)$$

and

$$\delta \Pi_{\lambda_T^{(p)}}^h(\mathbf{d}, A_T^{(p)}, \delta A_T^{(p)}) \equiv \int_{D^{(p)}} \delta A_T^{(p)} \bar{\mathbf{g}}_T^{(p)}(\mathbf{d}^{(D)}) dD$$

$$+ \int_{\Gamma_D^{(p)}} \delta A_T^{(p)} \tau^{(p)} (t_T(\mathbf{d}^{(z)}) - A_T^{(p)}) d\Gamma = 0$$

$$\forall \delta A_T^{(p)} \quad p \in \{1, \dots, n_T\}, \quad (90)$$

where $\Gamma_D^{(p)} = \partial D_n^{(p)} \cap \Gamma_D^{(z)}$ is the base-side of the patch (see Fig. 5) and a patch-wise constant value of the penalty multiplier $\tau \equiv \tau^{(p)}$ is considered. The solution of Eqs. (89) and (90) read:

$$\int_{D^{(p)}} \bar{\mathbf{g}}_N^{(p)} dD + \int_{\Gamma_D^{(p)}} \tau^{(p)} (t_N - A_N^{(p)}) d\Gamma = 0 \quad p \in \{1, \dots, n_N\} \quad (91)$$

and

$$\int_{D^{(p)}} \bar{\mathbf{g}}_T^{(p)} dD + \int_{\Gamma_D^{(p)}} \tau^{(p)} (t_T - A_T^{(p)}) d\Gamma = 0 \quad p \in \{1, \dots, n_T\}. \quad (92)$$

The integration of Eqs. (91) and (92) can be performed using

$$\int_{D^{(p)}} dD = \frac{1}{2} L^{(p)} H^{(p)} \quad \text{and} \quad \int_{\Gamma_D^{(p)}} d\Gamma = L^{(p)}, \quad (93)$$

where $L^{(p)}$ is the length of the base-side and $H^{(p)} = |\mathbf{g}_N^{(0)}(\mathbf{x}_3)|$ is the absolute value of the initial normal gap of the vertex node 3, that is, the height of the contact patch $D_n^{(p)}$ in the previous contact configuration (see Fig. 5).

If the normal and tangential stress measures t_N and t_T , obtained from the element adjacent to $D_n^{(p)}$ in the corresponding contacting body, are constant along the boundary $\Gamma_D^{(p)}$, utilizing Eq. (93) the integration of Eqs. (91) and (92) yields:

$$\frac{1}{2} H^{(p)} \bar{\mathbf{g}}_N^{(p)} + \tau^{(p)} (t_N - A_N^{(p)}) = 0 \quad p \in \{1, \dots, n_N\}$$

$$\frac{1}{2} H^{(p)} \bar{\mathbf{g}}_T^{(p)} + \tau^{(p)} (t_T - A_T^{(p)}) = 0 \quad p \in \{1, \dots, n_T\} \quad (94)$$

Remark 5-1. The assumption, that t_N and t_T are constant along the boundary $\Gamma_D^{(p)}$ is exact whenever the discretization of the contacting bodies is based on linear triangle finite elements. In fact, CST

(constant strain triangle) elements are utilized in the numerical implementation of the method done in this work (see Part 2 [12]). However, this does not imply a major restriction for the use of the present formulation. Indeed, if t_N and t_T are not constant along $\Gamma_D^{(p)}$, the integration of the variational constraint Eqs. (91) and (92) has to be performed numerically. Alternatively, a mean value of t_N and t_T along $\Gamma_D^{(p)}$ may be used.

Due to the use of linear triangular patches, the patch-wise constant gap intensities in Eq. (20) can be alternatively expressed with

$$\bar{\mathbf{g}}_N^{(p)} = \frac{\mathbf{g}_N(\mathbf{x}_3)}{|\mathbf{g}_N^{(0)}(\mathbf{x}_3)|} = \frac{(\mathbf{g}_N)_3}{H^{(p)}} \quad \text{and} \quad \bar{\mathbf{g}}_T^{(p)} = \frac{\mathbf{g}_T(\mathbf{x}_3)}{|\mathbf{g}_N^{(0)}(\mathbf{x}_3)|} = \frac{(\mathbf{g}_T)_3}{H^{(p)}}, \quad (95)$$

where $(\mathbf{g}_N)_3 = \mathbf{g}_N(\mathbf{x}_3)$ and $(\mathbf{g}_T)_3 = \mathbf{g}_T(\mathbf{x}_3)$ are the normal and tangential physical gaps for the vertex 3, respectively (see Fig. 5). Inserting Eq. (95) into Eq. (94) leads to the following numerical constraint equations:

$$\mathbf{g}_N^{num.(p)} = 0 \quad p \in \{1, \dots, n_N\}$$

$$\mathbf{g}_T^{num.(p)} = 0 \quad p \in \{1, \dots, n_T\} \quad (96)$$

with the definition of the numerical normal and tangential gaps:

$$\mathbf{g}_N^{num.(p)} \equiv (\mathbf{g}_N)_3 + 2\tau^{(p)} (t_N - A_N^{(p)}),$$

$$\mathbf{g}_T^{num.(p)} \equiv (\mathbf{g}_T)_3 + 2\tau^{(p)} (t_T - A_T^{(p)}). \quad (97)$$

Remark 5-2. The piece-wise constant numerical normal, $\mathbf{g}_N^{num.(p)}$, and tangential, $\mathbf{g}_T^{num.(p)}$, gaps in Eq. (97) are computed as the sum of the actual normal and tangential geometrical gaps $(\mathbf{g}_N)_3$ and $(\mathbf{g}_T)_3$ of the vertex 3 plus an additional term $(t_{N/T} - A_{N/T}^{(p)})$ penalized by the stabilization parameter $\tau^{(p)}$. A null value of $\tau^{(p)}$ will translate into numerical gaps equal to the geometrical gaps, and, therefore, into an exact imposition of the geometrical constraints. Additionally, mesh refinement will also make the penalized terms $(t_{N/T} - A_{N/T}^{(p)})$ tend to zero, according to Eq. (46), and, again, the numerical and geometrical gaps will coincide, regardless of the size of the penalty value $\tau^{(p)}$ (consistent penalty).

Remark 5-3. Notice that the final constraint Eq. (96) are independent of the value of the initial normal gap $\mathbf{g}_N^{(0)}(\mathbf{x}_n)$ in Eq. (17), which could eventually be null. In fact, the only relevant aspect for determination of the gap intensities in a given contact patch p is the connectivity of the three vertices (1,2,3) of the patch and the position of the projection of vertex 3 onto the base-side. This will be conveniently recalled for numerical implementation purposes in the second part of this work.

5.2.1. Effective gaps

With the definition of the numerical gaps in Eq. (97) and accounting for the discrete constraint Eq. (96), one can solve for the patch normal and tangential Lagrange multipliers as:

$$A_N^{(p)} = t_N + \frac{1}{2\tau^{(p)}} (\mathbf{g}_N)_3$$

$$A_T^{(p)} = t_T + \frac{1}{2\tau^{(p)}} (\mathbf{g}_T)_3 \quad (98)$$

where the role of $\tau^{(p)} > 0$ to allow for the, element by element, *lambda solvability* is clearly displayed. By multiplying Eq. (98) times $2\tau^{(p)}$ one gets the, from now on termed, *effective gaps*:

$$\begin{aligned} \mathbf{g}_N^{\text{eff.}(p)} &\equiv (\mathbf{g}_N)_3 + 2\tau^{(p)}\mathbf{t}_N = 2\tau^{(p)}A_N^{(p)}, \\ \mathbf{g}_T^{\text{eff.}(p)} &\equiv (\mathbf{g}_T)_3 + 2\tau^{(p)}\mathbf{t}_T = 2\tau^{(p)}A_T^{(p)}. \end{aligned} \quad (99)$$

Remark 5-4. The most relevant features of the effective gaps $\mathbf{g}_N^{\text{eff.}(p)}$ and $\mathbf{g}_T^{\text{eff.}(p)}$ defined in Eq. (99) are:

- Since $\tau^{(p)} > 0$ they have the same sign as the discrete Lagrange multipliers $A_N^{(p)}$ and $A_T^{(p)}$ i.e.:

$$\begin{aligned} \text{sign}(\mathbf{g}_N^{\text{eff.}(p)}) &= \text{sign}(A_N^{(p)}) \\ \text{sign}(\mathbf{g}_T^{\text{eff.}(p)}) &= \text{sign}(A_T^{(p)}) \end{aligned} \quad (100)$$

Therefore, they are *displacement-based* indicators of the sign of the Lagrange multipliers.

- They are constructed on basis of the values of the geometrical gaps, $(\mathbf{g}_N)_3$ and $(\mathbf{g}_T)_3$, and the contact (friction) tractions \mathbf{t}_N and \mathbf{t}_T . Due to this, they exhibit suitable *smoothness properties* along situations involving change of the contact/friction scenario, i.e.: contact-to-release and stick-to-slip. This fact will be crucially used in the specific algorithm for determining the active contact/friction sets (see also Remark 5-5 below).

5.3. Active constraint indicator

According to the definitions of the active domains $D_n^{(N)}$ and $D_n^{(T)}$ in Eqs. (49) and (50), the values of $A_N^{(p)}$ and $\Phi^{(p)}$ are used to decide, whether a patch p belongs to $D^{(N)}$ or to $D^{(T)}$, i.e.:

$$\begin{aligned} A_N^{(p)} < 0 &\iff D_n^{(p)} \subset D_n^{(N)} \rightarrow \text{active normal contact,} \\ \Phi^{(p)} < 0 &\iff D_n^{(p)} \subset D_n^{(T)} \rightarrow \text{active stick} \end{aligned} \quad (101)$$

Now, in view of Eq. (100), an *active normal contact patch* is given with

$$D_n^{(p)} \subset D_n^{(N)} \iff \begin{cases} A_N^{(p)} < 0, \\ \text{sign}(A_N^{(p)}) = \text{sign}(\mathbf{g}_N^{\text{eff.}(p)}) \end{cases} \iff \mathbf{g}_N^{\text{eff.}(p)} < 0. \quad (102)$$

Then, from the definition of Φ in Eq. (34) and with Eq. (99) an *active tangential stick contact patch* fulfills

$$\begin{aligned} D_n^{(p)} \subset D_n^{(T)} &\iff \Phi = |A_T^{(p)}| - \mu |A_N^{(p)}| < 0 \\ &\iff \frac{1}{2\tau^{(p)}} (|\mathbf{g}_T^{\text{eff.}(p)}| - \mu |\mathbf{g}_N^{\text{eff.}(p)}|) < 0 \\ &\iff |\mathbf{g}_T^{\text{eff.}(p)}| - \mu |\mathbf{g}_N^{\text{eff.}(p)}| < 0 \end{aligned} \quad (103)$$

where the fact that $\tau^{(p)} > 0$ has been considered. Finally from Eqs. (102) and (103) the following suitable (displacement-based) *active constraint indicators* β_N and β_T may be obtained:

$$\begin{aligned} D_n^{(p)} \subset D_n^{(N)} &\iff \beta_N \equiv \mathbf{g}_N^{\text{eff.}(p)} < 0 \rightarrow \text{active normal contact,} \\ D_n^{(p)} \subset D_n^{(T)} &\iff \beta_T \equiv |\mathbf{g}_T^{\text{eff.}(p)}| - \mu |\mathbf{g}_N^{\text{eff.}(p)}| < 0 \rightarrow \text{active stick} \end{aligned} \quad (104)$$

5.4. Iterative solution algorithm

The iterative solution algorithm, focussing on the update of the active contact set is shown in Box 1 for the current time step $[t_n, t_{n+1}]$. Herein $\mathbf{K}_T^*(\mathbf{d}^{(i)})$ and $\mathbf{G}^*(\mathbf{d}^{(i)})$ represent the global tangent stiffness matrix and the residual vector of the linearized, condensed system of equations (see Eqs. (85) and (86)) and $\mathbf{d}^{(i)}$ stands

for the nodal incremental displacement values at iteration i . Their specifications will be given in the second part of this work [12].

To accelerate the active set strategy algorithm, the update of the active contact set is performed within each step of the NEWTON iteration. The rate of convergence of the active contact set crucially depends on the appropriate prediction of the active set made in the first iteration. Therefore the active contact set in the first iteration is defined, computing the active constraint indicators on basis of a first order extrapolation of the values of the effective gaps of previous time steps:

$$\beta_N^{(1)} = \tilde{\mathbf{g}}_N^{\text{eff.}(p)} \quad \text{and} \quad \beta_T^{(1)} = |\tilde{\mathbf{g}}_T^{\text{eff.}(p)}| - \mu |\tilde{\mathbf{g}}_N^{\text{eff.}(p)}| \quad (105)$$

with

$$\tilde{\mathbf{g}}_{N/T}^{\text{eff.}(p)}(t_{n+1}) = \mathbf{g}_{N/T}^{\text{eff.}(p)}(t_n) + \frac{\Delta t_{n+1}}{\Delta t_n} \Delta \mathbf{g}_{N/T}^{\text{eff.}(p)}. \quad (106)$$

Herein Δt_{n+1} and Δt_n are the current and the previous time increments and $\Delta \mathbf{g}_{N/T}^{\text{eff.}(p)}$ are the effective normal and tangential gap increments

$$\Delta \mathbf{g}_{N/T}^{\text{eff.}(p)} = \mathbf{g}_{N/T}^{\text{eff.}(p)}(t_n) - \mathbf{g}_{N/T}^{\text{eff.}(p)}(t_{n-1}). \quad (107)$$

Box 1: Solution algorithm with active set strategy for one time step

```

LOOP over NEWTON ITERATION:  $i = 1, \dots, \text{convergence}$ 
  LOOP over all contact patches  $p$ 
    IF ( $i = 1$ ) THEN
      Define the ACTIVE SET based on extrapolated indicators
       $\beta_N^{(1)} = \tilde{\mathbf{g}}_N^{\text{eff.}(p)}$  and  $\beta_T^{(1)} = |\tilde{\mathbf{g}}_T^{\text{eff.}(p)}| - \mu |\tilde{\mathbf{g}}_N^{\text{eff.}(p)}|$ 
    ELSE IF ( $i > 1$ )
      Define the ACTIVE SET based on updated indicators
       $\beta_N^{(i)} = \beta_N(\mathbf{d}^{(i)})$  and  $\beta_T^{(i)} = \beta_T(\mathbf{d}^{(i)})$ 
    END IF
    IF  $\beta_N^{(i)} < 0$  THEN
       $D_n^{(p)} \subset D_n^{(N)}$ 
    ELSE IF  $\beta_T^{(i)} < 0$  THEN  $D_n^{(p)} \subset D_n^{(T)}$  ELSE  $D_n^{(p)} \subset D_n^{(N)} \setminus D_n^{(T)}$  END IF
    END IF
  END LOOP over contact patches
  Solve the equality constrained problem
   $\mathbf{K}_T^*(\mathbf{d}^{(i)}) \Delta \mathbf{d}^{(i)} = -\mathbf{G}^*(\mathbf{d}^{(i)})$ 
  Update incremental displacements
   $\mathbf{d}^{(i+1)} = \mathbf{d}^{(i)} + \Delta \mathbf{d}^{(i)}$ 
  Check for convergence:  $\|\mathbf{G}^*(\mathbf{d}^{(i+1)})\| \leq \text{TOL} \Rightarrow \text{STOP}$ 
  END LOOP over NEWTON ITERATION

```

Remark 5-5. Due to the smoothness of the effective gaps $\mathbf{g}_{N/T}^{\text{eff.}(p)}$ along the process (see Remark 5-4), their extrapolation provide good predictive properties. Thus, in many cases, the active set strategy part of the iteration algorithm in Box 1 converges in very few, if not in a unique, iterations.

6. Concluding remarks

Along this work, the theoretical aspects of a contact domain method for two-dimensional, large deformation, frictional contact problems have been presented. The presented approach displays some distinguishing features with respect to more classical ones, namely:

- The contact virtual work as well as the contact constraint equations are formulated on basis of a two-dimensional domain, called *contact domain*. This domain displays a unique, non-overlapping, pairing between the contacting boundaries and, as the simplest but not the unique possibility, is generated via a constrained Delaunay triangulation.
- The contact domain is endowed with a displacement field interpolated from the incremental displacements of the contacting boundaries. This allows the formulation of the geometrical contact constraints via dimensionless, strain-like quantities, called the normal and tangential gap intensities. They are defined for every point in the contact domain, and emerge to be constant within a linear triangular contact patch. Furthermore, the gap intensities, and their variation and linearization, can be expressed in terms of strain measures of the incremental motion of the contact patch.
- The contact constraint enforcement is based on a generalization of the stabilized Lagrange multiplier formulation, presented by Heintz and Hansbo [14] for small deformation, frictional contact problems. Starting from a classical Lagrange multiplier formulation, the variational constraint equations are enhanced with consistent stabilization terms, which allow for the condensation of the previously introduced Lagrange multipliers. As the stabilization terms involve the stress field at the boundaries of the contacting bodies, the resulting contact stiffness contributions will involve finite element nodes in the interior of the contacting bodies. This will be discussed in more detail in the second part of this work [12].
- The determination of the active contact/friction sets in the contact domain is made via an active set strategy. Therefore, the concept of effective gaps, as mechanical entities involving the geometrical gaps and the contact stresses, exhibiting suitable smoothness properties for predictive strategies, is introduced and used for such purpose.

For linear triangular patches, the method finally imposes the contact friction restrictions at the nodes of every triangular patch (see Eqs. (96) and (97)). In view of this one could wonder if the use of a contact domain method leads to the same results than a stabilized node-to-segment method or, in other words, if both methods are the same method written in a different format. Indeed, at the patch level, the contact restrictions for a linear triangular patch coincide with those of a (stabilized) node-to-segment contact element. However, the contact domain method as a general contact strategy provides some important differences, that stem from the approximation of the contact domain via a constraint Delaunay triangulation:

- The generation of contact patches is independent of the choice of a slave or a master side (see Fig. 2).
- The contact elements are uniquely defined, not suffering from possible problems involved when using the widely used closest point projection procedure [17].
- The contact domain is approximated with a full set of non-overlapping contact patches, that allows this method to pass the contact patch test for arbitrary non-conforming surface grids (see Part 2 of this work [12]).

In addition, when considered for 3D cases, the method seems to provide in a natural way pairing scenarios not considered in node-to-surface methods, e.g. that of a tetrahedron with one side at every contacting surface (see also Remark 2-6). These facts will be explored in a subsequent work.

Details on the numerical and implementation aspects of the approach, as well as numerical simulations and comparison studies

to prove its computational efficiency are provided in the second part of this work [12].

Acknowledgements

Financial support from the Spanish Ministry of Science and Technology, through grant BIA2005-09250-C03-03, and the Spanish Ministry of Science and Innovation, through grant BIA2008-00411 are gratefully acknowledged. The second author also acknowledges the support of the German Research Foundation through grant HA 5433–1-1.

Appendix A. Variations and linearizations

A.1. Variation and linearization of current tangent vector

Starting from Eq. (10)₁

$$\mathbf{t} = \frac{\mathbf{f} \cdot \mathbf{T}}{\beta} \quad \text{with } \beta = \|\mathbf{f} \cdot \mathbf{T}\| \quad (108)$$

and utilizing

$$\delta \mathbf{t} \cdot \mathbf{t} = 0 \iff \delta \mathbf{t} = \delta \gamma \mathbf{n} \quad (109)$$

the variation of the current tangent vector is derived with

$$\begin{aligned} \beta \mathbf{t} &= \mathbf{f} \cdot \mathbf{T} \\ \rightarrow \delta \beta \mathbf{t} + \beta \delta \mathbf{t} &= \delta \mathbf{f} \cdot \mathbf{T} \\ \rightarrow \delta \beta \underbrace{\mathbf{t} \cdot \mathbf{n}}_0 + \beta \underbrace{\delta \mathbf{t} \cdot \mathbf{n}}_{\delta \gamma} &= (\delta \mathbf{f} \cdot \mathbf{T}) \cdot \mathbf{n} \\ \rightarrow \delta \gamma &= \frac{1}{\beta} \mathbf{n} \cdot (\delta \mathbf{f} \cdot \mathbf{T}) = \frac{1}{\beta} \mathbf{n} \cdot \underbrace{\text{GRAD}(\delta \mathbf{u}) \cdot \mathbf{T}}_{\text{grad}(\delta \mathbf{u}) \cdot \mathbf{f}} \\ &= \frac{1}{\beta} \mathbf{n} \cdot \text{grad}(\delta \mathbf{u}) \cdot \underbrace{\mathbf{f} \cdot \mathbf{T}}_{\beta \mathbf{t}} = \mathbf{n} \cdot (\text{grad}(\delta \mathbf{u}) \cdot \mathbf{t}) \\ \Rightarrow \delta \mathbf{t} &= \delta \gamma \mathbf{n} = (\mathbf{n} \cdot \text{grad}(\delta \mathbf{u}) \cdot \mathbf{t}) \mathbf{n} = (\mathbf{n} \otimes \mathbf{n}) \cdot \frac{\partial \delta \mathbf{u}}{\partial \mathbf{t}}. \end{aligned} \quad (110)$$

As the linearization takes the same form as the variation:

$$\Delta \mathbf{t} = (\mathbf{n} \otimes \mathbf{n}) \cdot \frac{\partial \Delta \mathbf{u}}{\partial \mathbf{t}}. \quad (111)$$

A.2. Variation and linearization of current normal vector

From Eq. (10)₂ follows

$$\mathbf{n} = \mathbf{t} \times \hat{\mathbf{e}}_3 \Rightarrow \delta \mathbf{n} = \delta \mathbf{t} \times \hat{\mathbf{e}}_3 \quad \text{and} \quad \Delta \mathbf{n} = \Delta \mathbf{t} \times \hat{\mathbf{e}}_3 \quad (112)$$

and hence with (110) and (111)

$$\delta \mathbf{n} = -(\mathbf{t} \otimes \mathbf{n}) \cdot \frac{\partial \delta \mathbf{u}}{\partial \mathbf{t}} \quad \text{and} \quad \Delta \mathbf{n} = -(\mathbf{t} \otimes \mathbf{n}) \cdot \frac{\partial \Delta \mathbf{u}}{\partial \mathbf{t}}. \quad (113)$$

A.3. Variation of normal gap intensity

Starting from Eq. (20)₁

$$\begin{aligned} \bar{g}_N &= \text{sign}(g_N^{(0)}) \mathbf{n} \cdot \mathbf{f} \cdot \mathbf{N} \\ \Rightarrow \delta \bar{g}_N &= \text{sign}(g_N^{(0)}) (\delta \mathbf{n} \cdot \mathbf{f} \cdot \mathbf{N} + \mathbf{n} \cdot \delta \mathbf{f} \cdot \mathbf{N}) \end{aligned} \quad (114)$$

and using Eq. (113)

$$\delta \bar{g}_N = \text{sign}(g_N^{(0)}) \left[\mathbf{n} \cdot \underbrace{\text{GRAD}(\delta \mathbf{u}) \cdot \mathbf{N}}_{\text{grad}(\delta \mathbf{u}) \cdot \mathbf{f}} - \left(\mathbf{n} \cdot \frac{\partial \delta \mathbf{u}}{\partial \mathbf{t}} \right) \underbrace{(\mathbf{t} \cdot \mathbf{f} \cdot \mathbf{N})}_{\text{sign}(g_N^{(0)}) \bar{g}_T} \right]. \quad (115)$$

Using Eqs. (15) and (13)

$$\mathbf{g}(\mathbf{x}_n) = \mathbf{g}_N^{(0)} \mathbf{f} \cdot \mathbf{N} = \mathbf{g}_N(\mathbf{x}_n) \mathbf{n} + \mathbf{g}_T(\mathbf{x}_n) \mathbf{t}. \quad (116)$$

Leads to

$$\mathbf{f} \cdot \mathbf{N} = \frac{\mathbf{g}_N(\mathbf{x}_n)}{\mathbf{g}_N^{(0)}} \mathbf{n} + \frac{\mathbf{g}_T(\mathbf{x}_n)}{\mathbf{g}_N^{(0)}} \mathbf{t} = \text{sign}(\mathbf{g}_N^{(0)}) \bar{\mathbf{g}}_N \mathbf{n} + \text{sign}(\mathbf{g}_N^{(0)}) \bar{\mathbf{g}}_T \mathbf{t}. \quad (117)$$

Inserting (117) into (115) gives

$$\delta \bar{\mathbf{g}}_N = \bar{\mathbf{g}}_N \mathbf{n} \cdot \text{grad}(\delta \mathbf{u}) \cdot \mathbf{n}. \quad (118)$$

A.4. Variation of tangential gap intensity

Starting from Eq. (20)₂

$$\begin{aligned} \bar{\mathbf{g}}_T &= \text{sign}(\mathbf{g}_N^{(0)}) \mathbf{t} \cdot \mathbf{f} \cdot \mathbf{N} \\ \Rightarrow \delta \bar{\mathbf{g}}_T &= \text{sign}(\mathbf{g}_N^{(0)}) (\delta \mathbf{t} \cdot \mathbf{f} \cdot \mathbf{N} + \mathbf{t} \cdot \delta \mathbf{f} \cdot \mathbf{N}) \end{aligned} \quad (119)$$

using Eq. (110)

$$\delta \bar{\mathbf{g}}_T = \text{sign}(\mathbf{g}_N^{(0)}) \left[\mathbf{t} \cdot \underbrace{\text{GRAD}(\delta \mathbf{u}) \cdot \mathbf{N}}_{\text{grad}(\delta \mathbf{u}) \cdot \mathbf{f}} + \left(\mathbf{n} \cdot \frac{\partial \delta \mathbf{u}}{\partial \mathbf{t}} \right) \underbrace{(\mathbf{n} \cdot \mathbf{f} \cdot \mathbf{N})}_{\text{sign}(\mathbf{g}_N^{(0)}) \bar{\mathbf{g}}_N} \right] \quad (120)$$

and Eq. (117) gives

$$\delta \bar{\mathbf{g}}_T = \bar{\mathbf{g}}_N (\mathbf{n} \cdot \text{grad}(\delta \mathbf{u}) \cdot \mathbf{t} + \mathbf{t} \cdot \text{grad}(\delta \mathbf{u}) \cdot \mathbf{n}) + \bar{\mathbf{g}}_T \mathbf{t} \cdot \text{grad}(\delta \mathbf{u}) \cdot \mathbf{t}. \quad (121)$$

A.5. Linearization of the variation of the normal gap intensity

Starting from Eq. (118), the linearization reads

$$\Delta \delta \bar{\mathbf{g}}_N = \Delta \bar{\mathbf{g}}_N \mathbf{n} \cdot \frac{\partial \delta \mathbf{u}}{\partial \mathbf{n}} + \bar{\mathbf{g}}_N \Delta \mathbf{n} \cdot \frac{\partial \delta \mathbf{u}}{\partial \mathbf{n}} + \bar{\mathbf{g}}_N \mathbf{n} \cdot \Delta \left(\frac{\partial \delta \mathbf{u}}{\partial \mathbf{n}} \right), \quad (122)$$

where the linearization of the normal gap intensity has the same structure as Eq. (118)

$$\Delta \bar{\mathbf{g}}_N = \bar{\mathbf{g}}_N \mathbf{n} \cdot \text{grad}(\Delta \mathbf{u}) \cdot \mathbf{n} \quad (123)$$

and the linearization of the current normal vector is given in Eq. (113). The linearization of the n -directional derivative reads

$$\Delta \left(\frac{\partial \delta \mathbf{u}}{\partial \mathbf{n}} \right) = \Delta(\text{grad}(\delta \mathbf{u}) \cdot \mathbf{n}) = \Delta(\text{grad}(\delta \mathbf{u})) \cdot \mathbf{n} + \text{grad}(\delta \mathbf{u}) \cdot \Delta \mathbf{n} \quad (124)$$

with

$$\begin{aligned} \Delta(\text{grad}(\delta \mathbf{u})) &= \Delta(\text{GRAD}(\delta \mathbf{u}) \cdot \mathbf{f}^{-1}) = \underbrace{\text{GRAD}(\delta \mathbf{u})}_{\text{grad}(\delta \mathbf{u}) \cdot \mathbf{f}} \cdot \underbrace{\Delta \mathbf{f}^{-1}}_{-\mathbf{f}^{-1} \cdot \text{grad}(\Delta \mathbf{u})} \\ \Rightarrow \Delta(\text{grad}(\delta \mathbf{u})) &= -\text{grad}(\delta \mathbf{u}) \cdot \text{grad}(\Delta \mathbf{u}). \end{aligned} \quad (125)$$

Inserting (113) and (125) into (124) leads, after some standard algebraic transformations, to

$$\Delta \left(\frac{\partial \delta \mathbf{u}}{\partial \mathbf{n}} \right) = - \left(\frac{\partial \delta \mathbf{u}}{\partial \mathbf{n}} \right) \left(\mathbf{n} \cdot \frac{\partial \Delta \mathbf{u}}{\partial \mathbf{n}} \right) - \left(\frac{\partial \delta \mathbf{u}}{\partial \mathbf{t}} \right) \left(\mathbf{t} \cdot \frac{\partial \Delta \mathbf{u}}{\partial \mathbf{n}} + \mathbf{n} \cdot \frac{\partial \Delta \mathbf{u}}{\partial \mathbf{t}} \right). \quad (126)$$

Using this expression, the linearization of the variation of the normal gap intensity finally (Eq. (122)) reads

$$\begin{aligned} \Delta \delta \bar{\mathbf{g}}_N &= -\bar{\mathbf{g}}_N \left[\left(\mathbf{n} \cdot \frac{\partial \delta \mathbf{u}}{\partial \mathbf{t}} \right) \left(\mathbf{n} \cdot \frac{\partial \Delta \mathbf{u}}{\partial \mathbf{t}} \right) + \left(\mathbf{n} \cdot \frac{\partial \delta \mathbf{u}}{\partial \mathbf{t}} \right) \left(\mathbf{t} \cdot \frac{\partial \Delta \mathbf{u}}{\partial \mathbf{n}} \right) \right. \\ &\quad \left. + \left(\mathbf{t} \cdot \frac{\partial \delta \mathbf{u}}{\partial \mathbf{n}} \right) \left(\mathbf{n} \cdot \frac{\partial \Delta \mathbf{u}}{\partial \mathbf{t}} \right) \right]. \end{aligned} \quad (127)$$

A.6. Linearization of the variation of the tangential gap intensity

Starting from Eq. (121), the linearization reads

$$\begin{aligned} \Delta \delta \bar{\mathbf{g}}_T &= \Delta \bar{\mathbf{g}}_N \mathbf{n} \cdot \frac{\partial \delta \mathbf{u}}{\partial \mathbf{t}} + \bar{\mathbf{g}}_N \Delta \mathbf{n} \cdot \frac{\partial \delta \mathbf{u}}{\partial \mathbf{t}} + \bar{\mathbf{g}}_N \mathbf{n} \cdot \Delta \left(\frac{\partial \delta \mathbf{u}}{\partial \mathbf{t}} \right) \\ &\quad + \Delta \bar{\mathbf{g}}_T \mathbf{t} \cdot \frac{\partial \delta \mathbf{u}}{\partial \mathbf{n}} + \bar{\mathbf{g}}_T \Delta \mathbf{t} \cdot \frac{\partial \delta \mathbf{u}}{\partial \mathbf{n}} + \bar{\mathbf{g}}_T \mathbf{t} \cdot \Delta \left(\frac{\partial \delta \mathbf{u}}{\partial \mathbf{n}} \right) \\ &\quad + \Delta \bar{\mathbf{g}}_T \mathbf{t} \cdot \frac{\partial \delta \mathbf{u}}{\partial \mathbf{t}} + \bar{\mathbf{g}}_T \Delta \mathbf{t} \cdot \frac{\partial \delta \mathbf{u}}{\partial \mathbf{t}} + \bar{\mathbf{g}}_T \mathbf{t} \cdot \Delta \left(\frac{\partial \delta \mathbf{u}}{\partial \mathbf{t}} \right), \end{aligned} \quad (128)$$

where the linearization of the tangential gap intensity has the same structure as Eq. (121)

$$\Delta \bar{\mathbf{g}}_T = \bar{\mathbf{g}}_N (\mathbf{n} \cdot \text{grad}(\Delta \mathbf{u}) \cdot \mathbf{t} + \mathbf{t} \cdot \text{grad}(\Delta \mathbf{u}) \cdot \mathbf{n}) + \bar{\mathbf{g}}_T \mathbf{t} \cdot \text{grad}(\Delta \mathbf{u}) \cdot \mathbf{t} \quad (129)$$

and the linearization of the t -directional derivative reads

$$\Delta \left(\frac{\partial \delta \mathbf{u}}{\partial \mathbf{t}} \right) = \Delta(\text{grad}(\delta \mathbf{u}) \cdot \mathbf{t}) = \Delta(\text{grad}(\delta \mathbf{u})) \cdot \mathbf{t} + \text{grad}(\delta \mathbf{u}) \cdot \Delta \mathbf{t}. \quad (130)$$

Inserting (111) and (125) into (130) leads after some standard algebraic transformations to

$$\Delta \left(\frac{\partial \delta \mathbf{u}}{\partial \mathbf{t}} \right) = - \left(\frac{\partial \delta \mathbf{u}}{\partial \mathbf{t}} \right) \left(\mathbf{t} \cdot \frac{\partial \Delta \mathbf{u}}{\partial \mathbf{t}} \right). \quad (131)$$

Inserting this expression together with (123), (113), (111), (126), (129) into Eq. (128) leads finally to the linearization of the variation of the tangential gap intensity

$$\begin{aligned} \Delta \delta \bar{\mathbf{g}}_T &= \bar{\mathbf{g}}_N \left[\left(\mathbf{n} \cdot \frac{\partial \delta \mathbf{u}}{\partial \mathbf{t}} \right) \left(\mathbf{n} \cdot \frac{\partial \Delta \mathbf{u}}{\partial \mathbf{n}} \right) + \left(\mathbf{n} \cdot \frac{\partial \delta \mathbf{u}}{\partial \mathbf{n}} \right) \left(\mathbf{n} \cdot \frac{\partial \Delta \mathbf{u}}{\partial \mathbf{t}} \right) \right] \\ &\quad - \bar{\mathbf{g}}_N \left[\left(\mathbf{t} \cdot \frac{\partial \delta \mathbf{u}}{\partial \mathbf{t}} \right) \left(\mathbf{n} \cdot \frac{\partial \Delta \mathbf{u}}{\partial \mathbf{t}} \right) + \left(\mathbf{n} \cdot \frac{\partial \delta \mathbf{u}}{\partial \mathbf{t}} \right) \left(\mathbf{t} \cdot \frac{\partial \Delta \mathbf{u}}{\partial \mathbf{t}} \right) \right] \\ &\quad + \bar{\mathbf{g}}_T \left[\left(\mathbf{n} \cdot \frac{\partial \delta \mathbf{u}}{\partial \mathbf{t}} \right) \left(\mathbf{n} \cdot \frac{\partial \Delta \mathbf{u}}{\partial \mathbf{t}} \right) \right]. \end{aligned} \quad (132)$$

Appendix B. Quadratic triangular contact patch

In Fig. 7 a quadratic triangular contact patch is shown in the previous and current configuration. The initial gap for a specific particle $\mathbf{x}_n \in D_n^{(p)}$ is then calculated according to Eq. (11) in the previous configuration. Due to the motion of the contact patch, the necessary current normal and tangent vectors are given with

$$\begin{aligned} \mathbf{t} &= \mathbf{t}(\mathbf{x}_n) = \mathbf{t}(\bar{\mathbf{x}}_{n+1}), \\ \mathbf{n} &= \mathbf{n}(\mathbf{x}_n) = \mathbf{t}(\bar{\mathbf{x}}_{n+1}) \times \hat{\mathbf{e}}_3, \\ \bar{\mathbf{t}} &= \mathbf{t}(\bar{\mathbf{x}}_n) = \frac{\mathbf{f}(\bar{\mathbf{x}}_n) \cdot \mathbf{T}(\mathbf{x}_n)}{\|\mathbf{f}(\bar{\mathbf{x}}_n) \cdot \mathbf{T}(\mathbf{x}_n)\|}. \end{aligned} \quad (133)$$

The final gap vector $\mathbf{g}(\mathbf{x}_n)$ is then calculated using Eq. (12)

$$\mathbf{g} = \mathbf{g}(\mathbf{x}_n) = \mathbf{x}_{n+1} - \bar{\mathbf{x}}_{n+1} = \boldsymbol{\phi}^{(D)}(\mathbf{x}_n) - \boldsymbol{\phi}^{(D)}(\bar{\mathbf{x}}_n). \quad (134)$$

Due to the quadratic approximation of the base-side, the normal and tangential gaps can be calculated with (see Fig. 8)

$$\begin{aligned} g_N &= g_N(\mathbf{x}_n) = \mathbf{n} \cdot \mathbf{g} - a \\ g_T &= g_T(\mathbf{x}_n) \approx \mathbf{t} \cdot \mathbf{g} \left(1 + \frac{1}{2} (\mathbf{n} \cdot \bar{\mathbf{t}})^2 \right) \end{aligned} \quad (135)$$

with

$$2a = (\mathbf{n} \cdot \bar{\mathbf{t}}) (\mathbf{t} \cdot \mathbf{g}). \quad (136)$$

In Eq. (135)₂ some minor approximations have been used, that stem from the analytic integration of the curved length L (see Fig. 8) which is given with

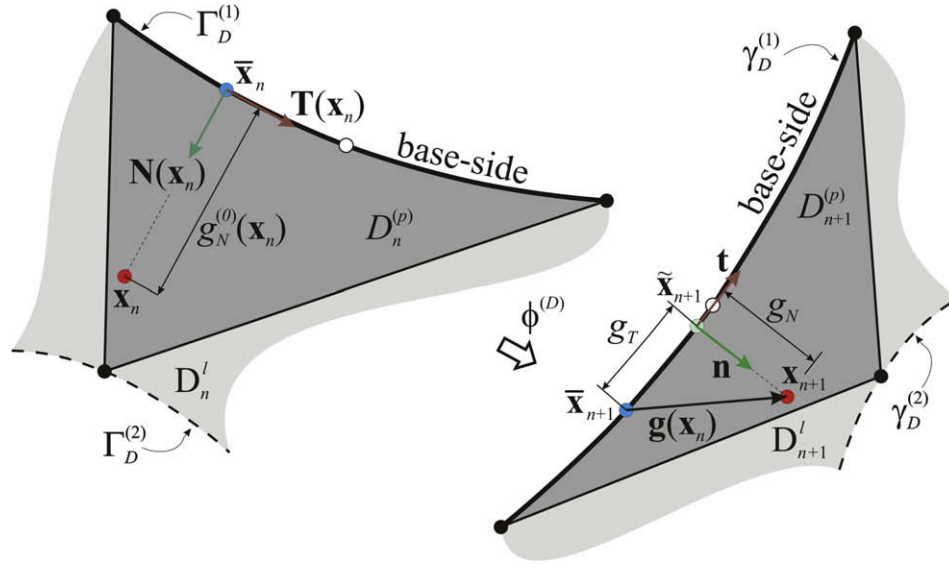


Fig. 7. Quadratic triangular contact patch in previous and current configuration.

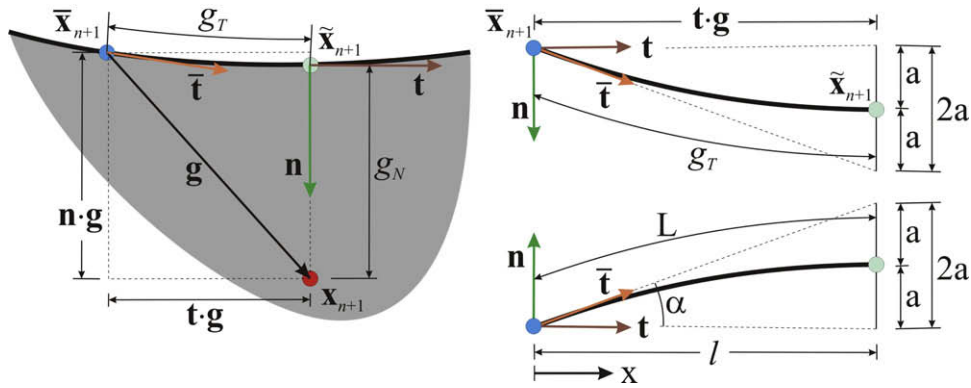


Fig. 8. Quadratic triangular contact patch: geometric gaps in current configuration.

$$L = \int_0^l \sqrt{1 + (f'(x))^2} dx \quad (137)$$

with

$$f(x) = -\frac{a}{l^2}x^2 + \frac{2a}{l}x \quad \text{and} \quad f'(x) = -\frac{2a}{l^2}x + \frac{2a}{l}. \quad (138)$$

The exact integration of (137) yields

$$L = \frac{l^2}{4a} \left[\frac{2a}{l} \sqrt{\left(\frac{2a}{l}\right)^2 + 1} + \ln \left(\frac{2a}{l} + \sqrt{\left(\frac{2a}{l}\right)^2 + 1} \right) \right]. \quad (139)$$

Inserting

$$a = \frac{1}{2}(\mathbf{n} \cdot \bar{\mathbf{t}})(\mathbf{t} \cdot \mathbf{g}) \quad \text{and} \quad l = \mathbf{t} \cdot \mathbf{g} \Rightarrow \frac{2a}{l} = (\mathbf{n} \cdot \bar{\mathbf{t}}). \quad (140)$$

Gives

$$g_T = \frac{\mathbf{t} \cdot \mathbf{g}}{2} \sqrt{(\mathbf{n} \cdot \bar{\mathbf{t}})^2 + 1} + \frac{\mathbf{t} \cdot \mathbf{g}}{2(\mathbf{n} \cdot \bar{\mathbf{t}})} \ln \left((\mathbf{n} \cdot \bar{\mathbf{t}}) + \sqrt{(\mathbf{n} \cdot \bar{\mathbf{t}})^2 + 1} \right). \quad (141)$$

For reasonable small changes between the two tangents \mathbf{t} and $\bar{\mathbf{t}}$ the following approximation can be introduced:

$$\mathbf{n} \cdot \bar{\mathbf{t}} = \sin \alpha; \quad \alpha = [\mathbf{t}, \bar{\mathbf{t}}] \quad (142)$$

$$\ln \left(\sin \alpha + \sqrt{(\sin \alpha)^2 + 1} \right) \approx \sin \alpha,$$

$$\sqrt{(\mathbf{n} \cdot \bar{\mathbf{t}})^2 + 1} + 1 \approx (\mathbf{n} \cdot \bar{\mathbf{t}})^2 + 2$$

which finally leads to the tangential gap in Eq. (135)₂. It can be shown, that the error, introduced by these two approximations is less than 5%, once the angle α within one quadratic triangular contact patch is smaller than 25°. Thus the gap intensities for a quadratic triangular contact patch are computed, dividing the definitions for the geometric gaps in Eq. (135) with the absolute value of the initial normal gap (see Eq. (17)).

$$\bar{g}_N(\mathbf{x}_n) = \frac{\mathbf{n}(\mathbf{x}_n) \cdot \mathbf{g}(\mathbf{x}_n) + \frac{1}{2}(\mathbf{t}(\mathbf{x}_n) \cdot \mathbf{g}(\mathbf{x}_n))(\mathbf{n}(\mathbf{x}_n) \cdot \mathbf{t}(\bar{\mathbf{x}}_n))}{|(\mathbf{x}_n - \bar{\mathbf{x}}_n) \cdot \mathbf{N}(\mathbf{x}_n)|}, \quad (143)$$

$$\bar{g}_T(\mathbf{x}_n) = \frac{\mathbf{t}(\mathbf{x}_n) \cdot \mathbf{g}(\mathbf{x}_n) + \frac{1}{2}(\mathbf{t}(\mathbf{x}_n) \cdot \mathbf{g}(\mathbf{x}_n))(\mathbf{n}(\mathbf{x}_n) \cdot \mathbf{t}(\bar{\mathbf{x}}_n))^2}{|(\mathbf{x}_n - \bar{\mathbf{x}}_n) \cdot \mathbf{N}(\mathbf{x}_n)|}$$

In contrast to the linear triangular contact patch discussed in Section 2.3, these gap intensities now vary within on quadratic triangular contact patch. Thus these values have to be evaluated at a number of quadrature points when performing the numerical integration.

Appendix C

Let us assume the proposition $D^{(T)} \cap D^{(N)} \neq D^{(T)}$. Therefore, from Eqs. (101) and (102) there should exist some \mathbf{x}_n such that:

$$\left. \begin{array}{l} \mathbf{x}_n \in D^{(T)} \Rightarrow \Phi(\mathbf{x}_n) < 0 \\ \mathbf{x}_n \notin D^{(N)} \Rightarrow \lambda_N(\mathbf{x}_n) = 0 \end{array} \right\} \Rightarrow |\lambda_T(\mathbf{x}_n)| - \mu|\lambda_N(\mathbf{x}_n)| = |\lambda_T(\mathbf{x}_n)| < 0 \quad (144)$$

which is not possible. Therefore

$$D^{(T)} \cap D^{(N)} = D^{(T)} \Rightarrow D^{(T)} \subset D^{(N)}. \quad (145)$$

References

- [1] D.N. Arnold, An interior penalty finite element method with discontinuous elements, *SIAM J. Numer. Anal.* 19 (1982) 742–760.
- [2] F. Belgacem, P. Hild, P. Laborde, The mortar finite element method for contact problems, *Math. Comput. Model.* 28 (1998) 263–271.
- [3] C. Bernardi, N. Debit, Y. Maday, Coupling finite elements and spectral methods: first results, *Math. Comput.* 54 (1990) 21–39.
- [4] C. Bernardi, Y. Maday, A. Patera, Domain decomposition by the mortar element method, in: H. Kasper, M. Garby (Eds.), *Asymptotic and Numerical Methods for Partial Differential Equations with Critical Parameters*, Kluwer Academic Publisher, Dordrecht, Netherlands, 1993, pp. 269–286.
- [5] C. Bernardi, Y. Maday, A. Patera, A new nonconforming approach to domain decomposition: the mortar element method, in: H. Brezis, J. Lions (Eds.), *Nonlinear Partial Differential Equations and their Applications – Collège de France Seminar*, vol. XI, Longman, Harlow, 1994, pp. 13–51.
- [6] J. Bonet, R.D. Wood, *Nonlinear Continuum Mechanics for Finite Element Analysis*, Cambridge University Press, Cambridge, UK, 1997.
- [7] N. El-Abbasi, K.-J. Bathe, Stability and patch test performance of contact discretizations and a new solution algorithm, *Comput. Struct.* 79 (2001) 1473–1486.
- [8] K.A. Fischer, P. Wriggers, Frictionless 2D Contact formulations for finite deformations based on the mortar method, *Comput. Mech.* 36 (2005) 226–244.
- [9] K.A. Fischer, P. Wriggers, Mortar based frictional contact formulation for higher order interpolations using the moving friction cone, *Comput. Methods Appl. Mech. Engrg.* 195 (2006) 5020–5036.
- [10] P.L. George, *Automatic Mesh Generation, Applications to Finite Methods*, Wiley, New York, 1991.
- [11] J. Hallquist, G. Goudreau, D. Benson, Sliding interfaces with contact-impact in large-scale Lagrangian computations, *Comput. Methods Appl. Mech. Engrg.* 51 (1985) 107–137.
- [12] S. Hartmann, J. Oliver, R. Weyler, J.C. Cante, J. Hernández, A contact domain method for large deformation frictional contact problems. Part 2: Numerical aspects, *Comput. Methods Appl. Mech. Engrg.* 198 (2009) 2607–2631.
- [13] A. Heege, P. Alart, A frictional contact element for strongly curved contact problems, *Int. J. Numer. Methods Engrg.* 39 (1996) 165–184.
- [14] P. Heintz, P. Hansbo, Stabilized Lagrange multiplier method for bilateral elastic contact with friction, *Comput. Methods Appl. Mech. Engrg.* 195 (2006) 4323–4333.
- [15] P. Hild, Numerical implementation of two nonconforming finite element methods for unilateral contact, *Comput. Methods Appl. Mech. Engrg.* 184 (2000) 99–123.
- [16] S. Hüeber, B. Wohlmuth, A primal–dual active set strategy for non-linear multibody contact problems, *Comput. Methods Appl. Mech. Engrg.* 194 (2005) 3147–3166.
- [17] A. Konyukhof, K. Schweizerhof, On the solvability of closest point projection procedures in contact analysis: analysis and solution strategy for surfaces of arbitrary geometry, *Comput. Methods Appl. Mech. Engrg.* 197 (2008) 3045–3056.
- [18] A. Montlaur, S. Fernandez-Mendez, A. Huerta, Discontinuous Galerkin methods for the Stokes equations using divergence-free approximations, *Int. J. Numer. Methods Fluids* 57 (2008) 1071–1092.
- [19] J. Nitsche, Über ein Variationsprinzip zur Lösung von Dirichlet-Problemen bei Verwendung von Teilräumen, die keinen Randbedingungen unterworfen sind, *Abh. Math. Univ. Hamburg* 36 (1971) 9–15.
- [20] P. Papadopoulos, R. Taylor, A mixed formulation for the finite element solution of contact problems, *Comput. Methods Appl. Mech. Engrg.* 94 (1992) 373–389.
- [21] G. Pietrzak, A. Curnier, Large deformation frictional contact mechanics: continuum formulation and augmented Lagrangian treatment, *Comput. Methods Appl. Mech. Engrg.* 177 (1999) 351–381.
- [22] M. Puso, T. Laursen, A mortar segment-to-segment contact method for large deformation solid mechanics, *Comput. Methods Appl. Mech. Engrg.* 193 (2004) 601–629.
- [23] M. Puso, T. Laursen, A mortar segment-to-segment frictional contact method for large deformations, *Comput. Methods Appl. Mech. Engrg.* 193 (2004) 4891–4913.
- [24] J. Simo, P. Wriggers, R. Taylor, A perturbed Lagrangian formulation for the finite element solution of contact problems, *Comput. Methods Appl. Mech. Engrg.* 50 (1985) 163–180.
- [25] J.C. Simo, T.A. Laursen, An augmented Lagrangian treatment of contact problems involving friction, *Comput. Struct.* (1992) 42.
- [26] B. Wohlmuth, R. Krause, Monotone methods on non-matching grids for non-linear contact problems, *SIAM J. Sci. Comput.* 25 (2003) 324–347.
- [27] P. Wriggers, Finite element algorithms for contact problems, *Arch. Comput. Methods Engrg.* 2 (1995) 1–49.
- [28] P. Wriggers, *Computational Contact Mechanics*, second ed., Springer, Berlin, Heidelberg, New York, 2006.
- [29] P. Wriggers, J.C. Simo, A note on tangent stiffness for fully nonlinear contact problems, *Commun. Appl. Numer. Methods* 1 (1985) 199–203.
- [30] P. Wriggers, G.A. Zavarise, formulation for frictionless contact problems using a weak form introduced by Nitsche, *Comput. Mech.* 41 (2008) 407–420.
- [31] B. Yang, T. Laursen, X. Meng, Two dimensional mortar contact methods for large deformation frictional sliding, *Int. J. Numer. Methods Engrg.* 62 (2005) 1183–1225.
- [32] G. Zavarise, P. Wriggers, A segment-to-segment contact strategy, *Math. Comput. Model.* 28 (1998) 497–515.
- [33] O.C. Zienkiewicz, R.L. Taylor, *The Finite Element Method*, Butterworth, Oxford UK, 2000.